



THE UNIVERSITY *of* EDINBURGH

Edinburgh Research Explorer

Expression of genes in the 16p11.2 locus during development of the human fetal cerebral cortex

Citation for published version:

Morson, S, Yang, Y, Price, D & Pratt, T 2021, 'Expression of genes in the 16p11.2 locus during development of the human fetal cerebral cortex', *Cerebral Cortex*, vol. 31, no. 9, pp. 4038–4052. <https://doi.org/10.1093/cercor/bhab067>

Digital Object Identifier (DOI):

[10.1093/cercor/bhab067](https://doi.org/10.1093/cercor/bhab067)

Link:

[Link to publication record in Edinburgh Research Explorer](#)

Document Version:

Peer reviewed version

Published In:

Cerebral Cortex

General rights

Copyright for the publications made accessible via the Edinburgh Research Explorer is retained by the author(s) and / or other copyright owners and it is a condition of accessing these publications that users recognise and abide by the legal requirements associated with these rights.

Take down policy

The University of Edinburgh has made every reasonable effort to ensure that Edinburgh Research Explorer content complies with UK legislation. If you believe that the public display of this file breaches copyright please contact openaccess@ed.ac.uk providing details, and we will remove access to the work immediately and investigate your claim.



1 **Expression of genes in the *16p11.2* locus during development of the human fetal cerebral**
2 **cortex.**

3

4 **Sarah Morson^{1,2}, Yifei Yang^{1,2}, David J. Price^{1,2}, Thomas Pratt^{1,2,3}**

5

6 ¹Simons Initiative for the Developing Brain,

7 ²Centre for Discovery Brain Sciences,

8 Hugh Robson Building, Edinburgh Medical School Biomedical Sciences, The University of

9 Edinburgh, Edinburgh, United Kingdom, EH8 9XD, United Kingdom.

10 ³Correspondence:

11 Thomas Pratt

12 t.pratt@ed.ac.uk

13 Tel: +44(0)1316503732

14 **Running Title: 16p11.2 gene expression during human corticogenesis**

15

16

17

18

19

20 **Abstract**

21 The 593 kbp *16p11.2* copy number variation (CNV) affects the gene dosage of 29 protein coding
22 genes, with heterozygous *16p11.2* microduplication or microdeletion implicated in about 1% of
23 autism spectrum disorder (ASD) cases. The *16p11.2* CNV is frequently associated with
24 macrocephaly or microcephaly indicating early defects of neurogenesis may contribute to
25 subsequent ASD symptoms, but it is unknown which *16p11.2* transcripts are expressed in
26 progenitors and whose levels are likely, therefore, to influence neurogenesis. Analysis of human
27 fetal gene expression data revealed that *KIF22*, *ALDOA*, *HIRIP3*, *PAGRI*, and *MAZ* transcripts
28 are expressed in neural progenitors with *ALDOA* and *KIF22* significantly enriched compared to
29 post-mitotic cells. To investigate the possible roles of *ALDOA* and *KIF22* proteins in human
30 cerebral cortex development we used immunohistochemical staining to describe their expression
31 in late first and early second trimester human cerebral cortex. *KIF22* protein is restricted to
32 proliferating cells with its levels increasing during the cell cycle and peaking at mitosis. *ALDOA*
33 protein is expressed in all cell types and does not vary with cell-cycle phase. Our expression
34 analysis suggests the hypothesis that altered neurogenesis in the cerebral cortex contributes to ASD
35 in *16p11.2* CNV patients.

36

37 **Keywords:**

38 **ALDOA, Autism, Cerebral Cortex, CNV, KIF22**

39

40

41 **Introduction.**

42 Large, recurrent Copy Number Variations (CNVs) are implicated in many neuropsychiatric
43 disorders including autism spectrum disorders (ASD), epilepsy, intellectual disability (ID) and
44 schizophrenia (McCarthy *et al.*, 2009; Girirajan and Eichler, 2010; Levy *et al.*, 2011; Sanders *et*
45 *al.*, 2011; Malhotra and Sebat, 2012). The *16p11.2* CNV (OMIM 611913) encompasses a 593 kb
46 DNA sequence in the p11.2 region of human chromosome 16 (BP4-BP5). This region harbors 29
47 protein coding genes and is strongly linked to neurodevelopmental disorders (NDDs) including
48 ASD (Kumar *et al.*, 2008; Bijlsma *et al.*, 2009; Rosenfeld *et al.*, 2010; Shinawi *et al.*, 2010;
49 Zufferey *et al.*, 2012). This *16p11.2* region is flanked by two homologous 147kbp sequences that
50 arose after the evolutionary divergence of humans from other primates, generating a hot-spot for
51 mis-aligned recombination that explains the high frequency of the *16p11.2* CNV in the human
52 population and also the high frequency of *de novo* *16p11.2* CNV (Nuttle *et al.*, 2016). In humans,
53 the *16p11.2* microdeletion is associated with transient infant brain overgrowth (macrocephaly) and
54 focal thickening of the cerebral cortex, while the *16p11.2* microduplication is associated with
55 reduced brain size (microcephaly) (Qureshi *et al.*, 2014; Blackmon *et al.*, 2018). The early
56 manifestation of anatomical phenotype in newborns, along with the onset of ASD symptoms in
57 infancy, suggests crucial roles for *16p11.2* genes during neural development. *16p11.2* is the most
58 prevalent CNV associated with ASD, ~1% incidence, making this CNV particularly intriguing and
59 providing motivation for investigating the role played by *16p11.2* genes in brain development and
60 function (Weiss *et al.*, 2008). Available lines of evidence from *16p11.2* rodent models, *16p11.2*
61 patient derived lymphoblastoid cell lines, and human induced pluripotent stem cells genetically
62 engineered to harbor the *16p11.2* CNV indicate that all *16p11.2* mRNAs' levels reflect the altered
63 gene dosage of *16p11.2* genes (50% in microdeletion and 150% in microduplication

64 heterozygotes) (Horev *et al.*, 2011; Blumenthal *et al.*, 2014; Pucilowska *et al.*, 2015; Tai *et al.*,
65 2016). This indicates that multiple *16p11.2* transcript levels are affected by the *16p11.2* CNV and
66 that the pathology of the *16p11.2* CNV could stem from altered dosage of one or more them.

67 While none of the individual *16p11.2* genes have been identified as sole causative genes for the
68 *16p11.2* phenotype, *MAPK3*, *QPRT*, *KCTD13*, *ALDOA*, *TAOK2*, and *KIF22* have each been
69 individually associated with a variety of neural phenotypes in non-human models. These include
70 cell proliferation, neuronal morphology, axonal projection and spine morphogenesis, altered head
71 size, and behavioral phenotypes (Blaker-Lee *et al.*, 2012; de Anda *et al.*, 2012; Golzio *et al.*, 2012;
72 Pucilowska *et al.*, 2015, 2018) (Escamilla *et al.*, 2017) (Richter *et al.*, 2019) (Yadav *et al.*, 2017)
73 (Ultanir *et al.*, 2014).

74 The cellular mechanisms by which the *16p11.2* CNV cause the patient phenotype are poorly
75 understood. One plausible hypothesis is that disrupted neurogenesis causes changes in neuronal
76 output which produce a brain with abnormal cell number or composition and that this contributes
77 to the *16p11.2* pathology. Consistent with this hypothesis, the *16p11.2* deletion mouse model
78 exhibits proliferation defects in cortical progenitors during pre-natal brain development and
79 subsequently develops ASD-like symptoms (Horev *et al.*, 2011; Pucilowska *et al.*, 2015).
80 However, it is unknown which of the proteins produced by *16p11.2* CNV genes are expressed by
81 progenitor cells in the developing human cerebral cortex and are therefore candidates for
82 regulating neurogenesis.

83 Excitatory (glutamatergic) neurons in the human cerebral cortex are derived from progenitors that
84 reside in the ventricular and subventricular zones of the dorsal telencephalon while inhibitory
85 (GABAergic) interneurons are derived from progenitors that reside in the ventral telencephalon

86 and migrate into the cerebral cortex (Clowry et al., 2010) (Bystron et al., 2008) (Ma et al., 2013)
87 Here we focused on the potential for the *16p11.2* CNV to affect neurogenesis of excitatory neurons
88 in the developing human cerebral cortex by identifying *16p11.2* genes that are highly expressed in
89 cerebral cortex progenitors in the ventricular zones and down-regulated as cells become post-
90 mitotic. We analysed previously published human fetal cortex single cell RNA sequencing
91 (scRNA-seq) data (Pollen *et al.*, 2015) (Zhong et al., 2018) to identify candidate genes and
92 characterize their expression in sections of developing human fetal cerebral cortex from the late
93 first and early second trimester.

94

95 **Material and Methods**

96 **Human Tissue**

97 Human embryos ranging in age from 12-16 post-conceptual weeks (PCW) were obtained from
98 the MRC/Wellcome-Trust funded Human Developmental Biology Resource at Newcastle
99 University (HDBR, <http://www.hdbr.org/>) with appropriate maternal written consent and
100 approval from the Newcastle and North Tyneside NHS Health Authority Joint Ethics Committee.
101 HDBR is regulated by the UK Human Tissue Authority (HTA; www.hta.gov.uk) and operates in
102 accordance with the relevant HTA Codes of Practice.

103 For cryosections 12 PCW week brains were fixed in 4%PFA/PBS for 1 week then cryoprotected
104 with 30% sucrose/PBS and then embedded in 50:50 30% sucrose:OCT, flash frozen and
105 sectioned at 12µm using a Leica Cryostat.

106 Stages used for t study: 12 PCW (2 brains), 14 PCW (1 brain) and 16 PCW (1 brain).

107 **scRNA-seq Analysis**

108 The publicly available scRNA-seq data sets (Pollen *et al.*, 2015) (Zhong *et al.*, 2018) were used
109 to identify candidate genes. Prior to dataset publication the reads were aligned, we normalized
110 the RPKMs as $\log(x+1)$. Analysis was performed using R studio. To determine genes with
111 significant changes a Wilcox test by *FindAllMarkers* in Seurat package was used. Monocle2 R
112 package was used to order cells in pseudotime. To identify cell-cycle phase specific transcripts
113 we used function *CellCycleScoring* from Seurat R package.

114 **Immunohistochemistry**

115 Immunohistochemistry was carried out on paraffin sections obtained from HDBR. Antigen
116 retrieval consisting of boiling sections in 10mM sodium citrate pH6 for 10 mins was used for all
117 stains. Primary antibodies were diluted in 20% blocking serum in pH7.6 Tris buffered saline
118 (TBS) and sections incubated overnight at 4°C. Primary antibodies used: KID 1/5000 DAB,
119 1/2000 fluorescent (Invitrogen PA5-29490), KI67 1/800 (Novus Biologicals NBP2-22112),
120 ALDOA 1/100 (Sigma HPA004177).

121 For colourmetric stains, sections were incubated 1hr at room temperature with biotinylated
122 secondary antibody (1/200) followed by incubation for 1 hour with ABC (Vector Labs) and
123 developed with diaminobenzidine solution (Vector Labs), washed, counterstained with nuclear
124 fast red, dehydrated and then mounted using DPX.

125 For immunofluorescence sections were incubated with secondary antibodies 1/200 1 hour room
126 temperature, counterstained with 4',6-diamidino-2-phenylindole dihydrochloride
127 (DAPI;ThermoFisher) and mounted with Vectashield H1400 Hardset Mounting Medium (Vector

128 Labs). Extensive TBS washes were carried out between each step.

129 ***In Situ* Hybridisation**

130 PCR primers used to clone *in situ* probes from human cDNA into pGEMTeasy for preparation of
131 DIG labelled RNA were as follows: *ALDOA*, CTG TCA CTG GGA TCA CCT T, & GTG ATG
132 GAC TTA GCA TTC AC; *KIF22*,: CGA GAG CGG ATG GTG CTA AT &: GAG ACC CAG
133 GAT GTT TGC CT; *PAGRI*, ATG ATG AGC CAG TGA CAC CA & TCT GCC TCT CCC
134 TTC AAG TG; *HIRIP3*, TGG TGC CCA TCG AAA CTA CA & TGG CCC AAA ATA CAG
135 GAG GT; & *MAZ*, CAC GAG GAG AAA GTG CCA TG & GAG AGA AGA GGA CCG TCG
136 AG.

137 *In situ* hybridisation was performed on cryosections of 12 PCW brain as described previously
138 (Radonjić *et al.*, 2014). Briefly, 12µm cryosections were dried at 37°C for 3 hours then incubated
139 overnight at 70°C in hybridization mix containing 1x salts (200mM NaCl, 10mM Tris HCl (pH
140 7.5), 1mM Tris Base, 5mM NaH₂PO₄·2H₂O, 5mM Na₂HPO₄, 0.5M EDTA: Sigma-Aldrich), 50%
141 deionized formamide, 10% dextran sulfate, 1mg/ml rRNA, 1x Denhardt's, and DIG-labelled
142 RNA probe. Next day sections were washed 3 times at 70°C in wash buffer comprising 1x SSC,
143 50% formamide, 0.1% Tween-20 and then 3 times at RT in 1x MABT (20mM Maleic acid,
144 30mM NaCl, 0.5% Tween-20 and pH adjusted to 7.5 with 10mM NaOH). Sections were
145 incubated 1hr RT in 1x MABT blocking solution (20% sheep serum, 2% blocking reagent) and
146 then incubated overnight with anti-DIG antibody 1:1500 in blocking solution at 4°C followed by
147 colour reaction overnight at RT.

148 **Microscopy and Imaging**

149 DAB and *in situ* hybridisation images were taken using a Leica DMNB microscope with an
150 attached Leica DFC480 Camera. Fluorescence images were obtained with a Leica DM5500B
151 epifluorescence microscope with a DFC360FX camera. Confocal images were obtained using
152 Nikon A1R FILM microscope and analysed in ImageJ.

153 **Image Analysis and Quantification**

154 For DAB stains and *in situ* hybridisation the images were stitched in ImageJ using the stitching
155 plugin (Preibisch, Saalfeld and Tomancak, 2009).

156 For KIF22 analysis of DAB stains rectangular counting boxes (34x88 μ m) were overlaid across
157 the section. Using ImageJ cell counting plugin cells in each box were counted and denoted
158 KIF22+ (brown) or KIF22- (red). The distinction between the regions (VZ, SVZ, IZ/CP) was
159 determined anatomically by cell density. The count for each box was averaged with other boxes
160 in the region to provide the final value.

161 For analysis of KIF22/KI67 double staining counting boxes (20x145 μ m) were overlaid over the
162 VZ and SVZ (determined based on cell density). For determining intensity cells were randomly
163 selected on the DAPI channel, the nucleus outlined and intensity of KIF22 and KI67 recorded.
164 20 cells were selected per box and the counts from individual boxes combined to give final
165 values.

166 For subcellular ALDOA analysis counting boxes (20x145 μ m) were overlaid over the VZ and
167 SVZ. Cells were randomly selected on the DAPI channel, far enough apart to ensure their
168 cytoplasm would not overlap, the Z plane through the center of the cell was used and the nucleus
169 outlined. The KI67 and ALDOA intensity was measured constituting the nuclear value. To

170 obtain ALDOA cytoplasmic intensity the nuclear outline was duplicated and extended 4 pixels
171 allowing a reading of just the cytoplasmic area to be obtained (see Fig.6e). This was performed
172 for 10 cells in each box and the counts from individual boxes combined to give final values.

173 **Data Analysis and Statistics**

174 Where error bars are shown they are expressed as mean \pm SEM. Boxplots show median and upper
175 and lower quartiles. Statistical comparison between two groups was performed with a *t* test.
176 Statistical comparison between more than two groups was performed with ANOVA followed by
177 *post hoc* test. $P < 0.05$ was considered statistically significant. Analysis was performed using
178 GraphPad Prism.

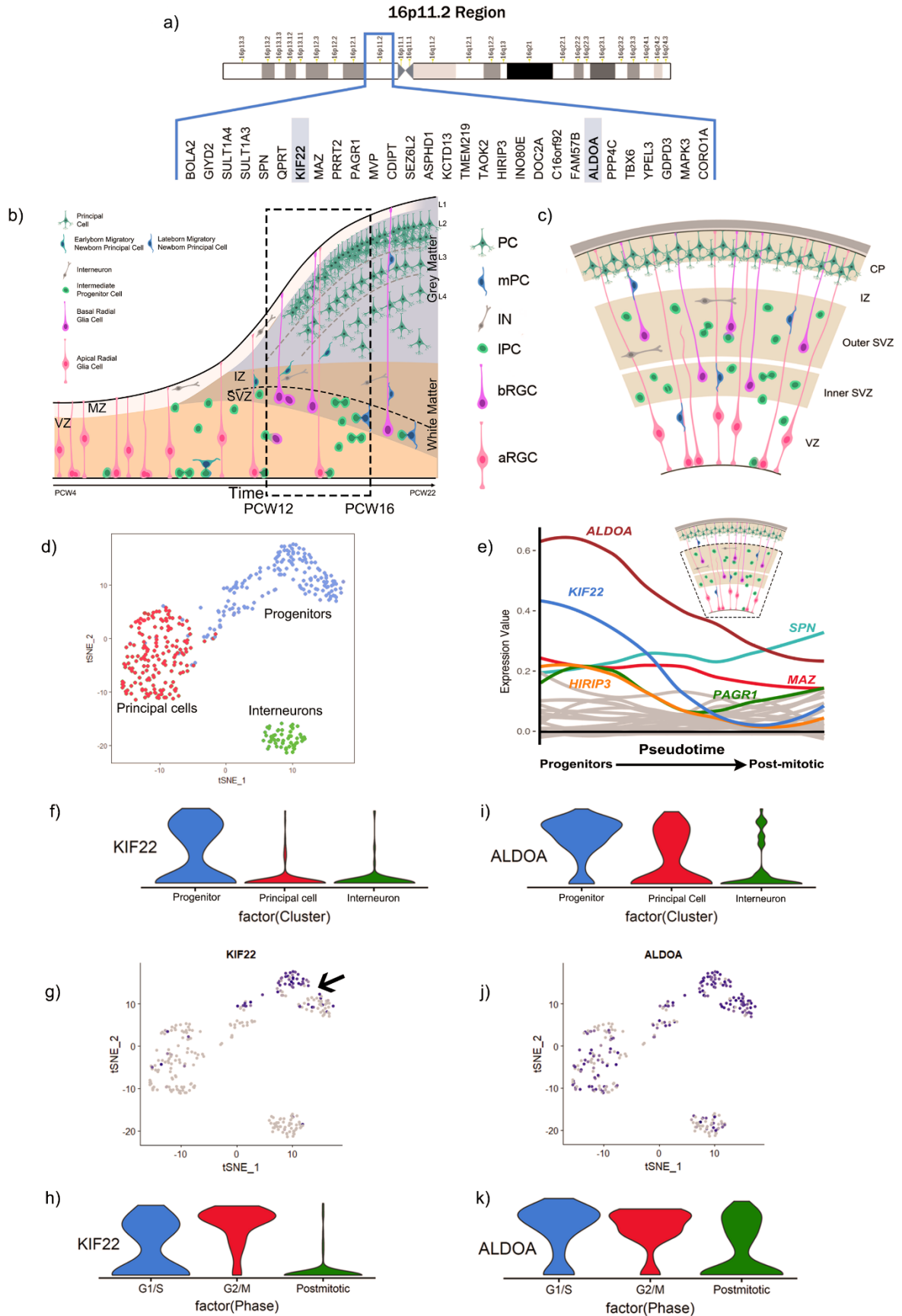
179

180 **Results**

181 **Analysis of scRNA-seq data identifies *KIF22* and *ALDOA* as progenitor-enriched *16p11.2*** 182 **transcripts in the developing human fetal cerebral cortex.**

183 The *16p11.2* CNV involves microduplication or microdeletion of a 593kb locus on human
184 chromosome 16 containing 29 protein coding genes (Fig.1a). The aim of the current study is to
185 identify *16p11.2* genes which are potential candidates for being involved in neurogenesis in the
186 developing human cerebral cortex (Fig.1b,c) and whose altered dosage in *16p11.2* microdeletion
187 or microduplication patients may disrupt neurogenesis and contribute to the CNV phenotype. We
188 reasoned that *16p11.2* genes important for neurogenesis would be highly expressed in proliferating
189 progenitor cells and down-regulated as cells became post-mitotic.

190



192 **Figure 1: Bioinformatics analysis of scRNA-seq from the VZ and SVZ of the 16-18GW**
193 **human fetal cortex.** a) 16p11.2 region and genes. b) schematic adapted from Budday et al 2015
194 shows the process of human fetal cortex development over time. Dotted box indicates
195 approximately the time-period of interest for our study; 12-16PCW. c) schematic of human
196 cortical structure during development. d) tSNE clustering of cell types. e) changing mRNA
197 expression levels of *16p11.2* genes as cells move from progenitors to neurons with *KIF22* and
198 *ALDOA* transcripts identified as changing significantly. Schematic of human cortex with dotted
199 box indicates the compartments of the brain that were used to generate this dataset – the
200 germinative VZ and SVZ. f) Violin plots showing distribution of *KIF22* in different cell types. g)
201 *KIF22* gradient plot (arrow indicates progenitors with a subset expressing high levels of *KIF22*
202 mRNA). h) Violin plots showing distribution of *KIF22* at different cell cycle stages. i) Violin
203 plots showing distribution of *ALDOA* mRNA levels in different cell types. j) *ALDOA* gradient
204 plot. k) Violin plots showing distribution of *ALDOA* mRNA at different cell cycle stages.

205

206 We took advantage of a published single cell RNA-sequencing (scRNA-seq) data-set acquired
207 from 393 cells of the ventricular zone (VZ) and subventricular zone (SVZ) of gestational week
208 (GW) 16-18 human fetal cerebral cortex (equivalent to post conception week (PCW) 14-16) to
209 perform an unbiased screen to identify *16p11.2* transcripts that matched this expression profile
210 (Pollen *et al.*, 2015). Dimensional reduction of the scRNA-seq data separated the cells into three
211 clusters based on transcriptome similarity (Fig.1d – each dot on the tSNE plot represents an
212 individual cell) that were subsequently identified as the three cardinal cell classes of progenitors
213 (blue), post-mitotic neurons/ principal cells (red) and interneurons (green), by expression of cell-
214 type specific transcripts. We next used the monocle2 R package to order the cells in pseudotime

215 using the normalized expression levels of selected differentially expressed genes (DEGs) as input
216 to order the cells (Trapnell *et al.*, 2014; Qiu *et al.*, 2017) (Fig.1e) moving from the progenitor state
217 (left) to post mitotic state (right) along the X-axis. We plotted the average expression of each
218 *16p11.2* transcript at each pseudotime-point on the Y-axis. We found that two genes, *KIF22* (blue
219 line) and *ALDOA* (brown line), were notable for having high expression in progenitors that
220 declined as cells became post-mitotic. A Wilcox test identified *ALDOA* and *KIF22* as the only
221 *16p11.2* transcripts that were significantly higher in progenitor than neuronal populations
222 ($p < 0.05$). Although not significantly enriched in progenitors *HIRIP3* (orange line), *MAZ* (red
223 line), *PAGR1* (green line) were expressed in progenitors at higher levels than the remaining
224 *16p11.2* transcripts (shown as grey lines), many of which were barely expressed at all.

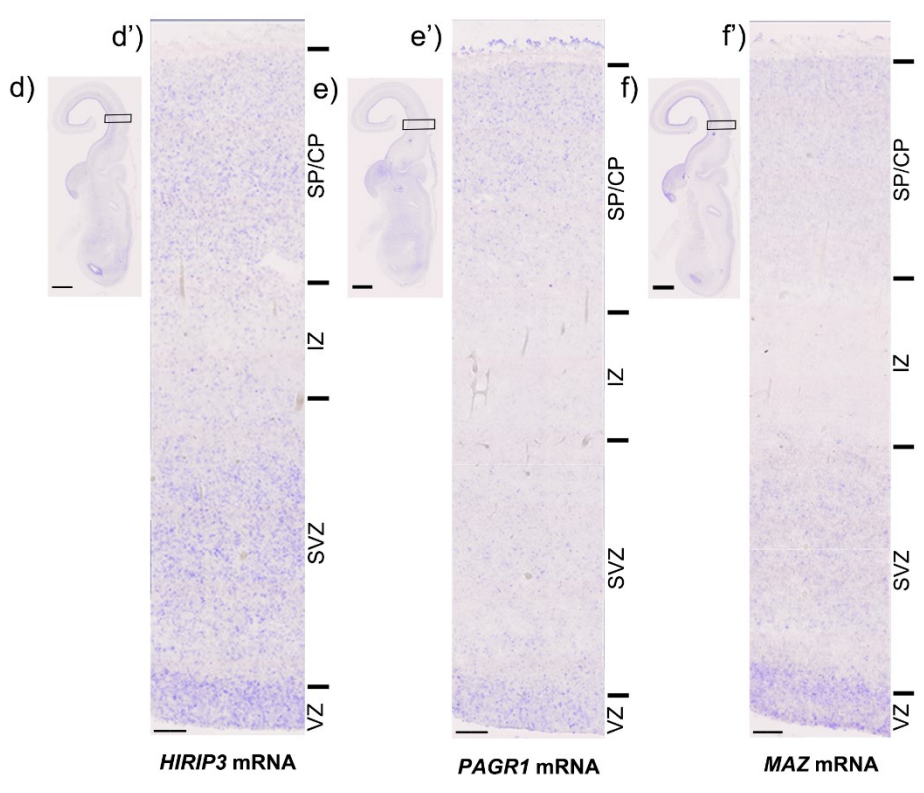
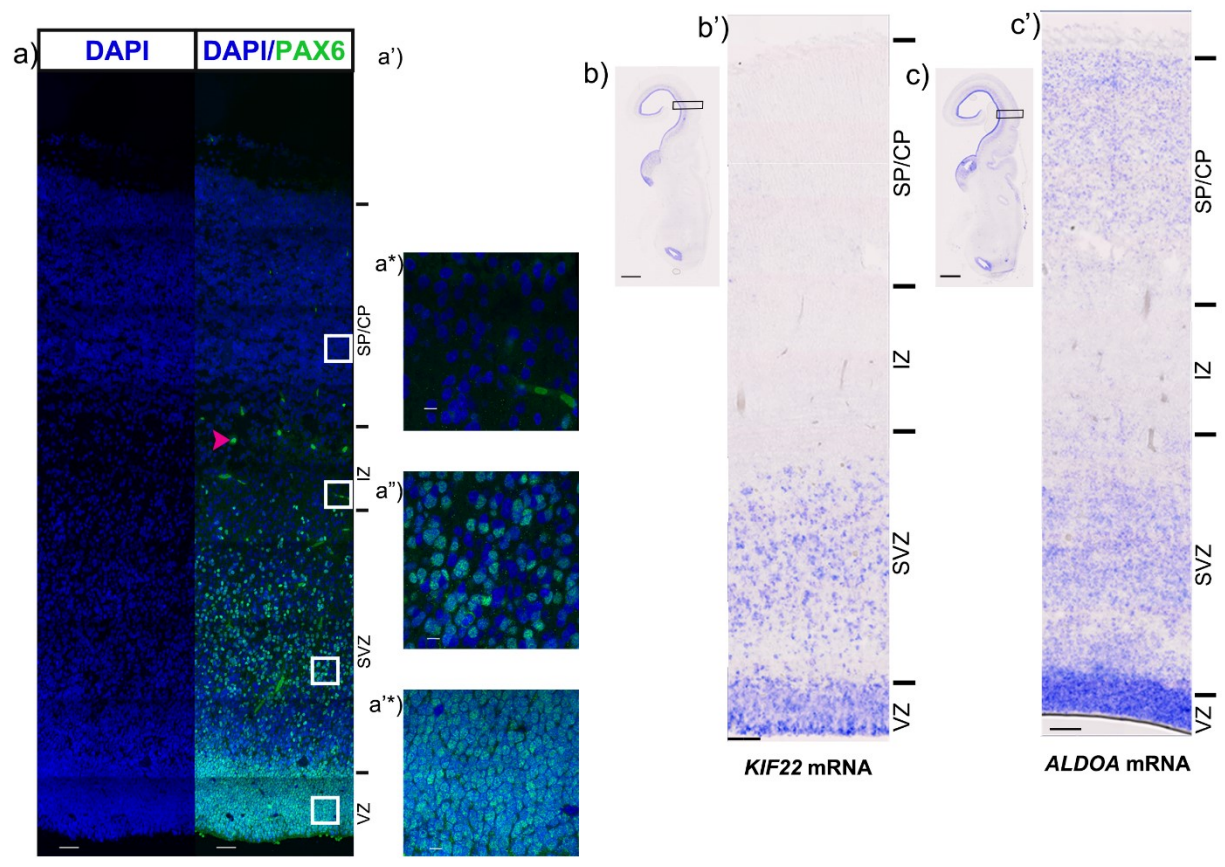
225 Violin plots of the numbers of cells expressing different levels of *KIF22* mRNA in the different
226 cardinal cell classes show that *KIF22* is expressed predominantly in progenitors (Fig.1f) and
227 mapping the expression level of *KIF22* onto the tSNE plot (Fig.1g) revealed that *KIF22* expression
228 is highest in a subset of the progenitor cluster (arrow in Fig.1g) with a substantial proportion of
229 progenitor cells expressing relatively low levels of *KIF22*. Very few post-mitotic neurons, both
230 interneurons and principal cells, express appreciable levels of *KIF22* (Fig.1f,g). The expression of
231 *KIF22* in a subset of progenitors prompted us to ask whether its expression was related to the cell-
232 cycle phase. We used the expression of cell-cycle phase specific transcripts using function
233 CellCycleScoring from Seurat R package to divide the cells into three classes (Macosko *et al.*,
234 2015; Tirosh *et al.*, 2016), G1/S, G2/M, and post-mitotic neurons, and compared *KIF22* transcript
235 levels between these three groups using a violin plot (Fig.1h). We found that the majority of cells
236 in G2/M phase expressed higher levels of *KIF22* (red plot), cells in G1/S expressed lower levels
237 (blue plot) while the vast majority of post-mitotic cells expressed low levels of *KIF22* (green plot).

238 Similar analysis for *ALDOA* show that while a greater proportion of cells expressing the highest
239 levels of *ALDOA* are progenitors (blue plot) there are also a substantial number of principal cells
240 (red plot) expressing similarly high levels of *ALDOA* transcripts although very few interneurons
241 (green plot). Mapping *ALDOA* expression level onto the tSNE plot (Fig.1j) shows cells expressing
242 high levels of *ALDOA* are evenly distributed throughout the progenitor cluster with appreciable
243 numbers of principal cells expressing high levels of *ALDOA* and a much lower proportion of
244 interneurons. In contrast to *KIF22*, there is no clear difference in the partitioning of *ALDOA*
245 expression level between different phases of the cell-cycle (Fig.1k). We performed the same
246 analysis on another developing human cortex scRNAseq data set that spanned a wider
247 developmental interval (PCW10-28) and also included cells from all layers of the cerebral cortex
248 (Zhong et al., 2018). This analysis produced similar results. *KIF22* transcripts showing them to be
249 enriched in progenitors (Sup Fig. 1b,e) and in G2/M phase of the cell cycle (Sup Fig.1g). Although
250 *ALDOA* transcript levels were highest in progenitors they did not decline as much as *KIF22* (Sup
251 Fig.1b,f) in postmitotic cells and showed no clear difference between different phases of the cell-
252 cycle (Sup Fig.1h).

253 We next used in situ hybridisation to visualise the expression of *KIF22*, *ALDOA*, *HIRIP3*, *PAGRI*,
254 and *MAZ* transcripts in the different layers of the 12 PCW brain. We identified the VZ and SVZ
255 based on cytoarchitecture, however, to validate our delineation we stained a section with PAX6,
256 expressed by progenitor cells (Fig.2a-a'*). This confirmed the absence of progenitor cells in the
257 IZ and CP and allowed us a guidance for estimating cellular location in other sections.

258 Consistent with the scRNAseq data *KIF22* and *ALDOA* transcripts are the most clearly
259 differentially expressed between zones containing progenitors (VZ and SVZ) and the more
260 superficial layers that are mainly composed of postmitotic cells (IZ and SP/CP). *KIF22* mRNA

261 expression is most prominent in the VZ and SVZ with a few expressing cells in the IZ and SP/CP
262 (Fig.2b and 2b') While *ALDOA* mRNA expression is most prominent in the proliferative VZ and
263 SVZ there are substantial numbers of *ALDOA* expressing cells in the SP/CP (Fig.2c and 2c').
264 *HIRIP3* (Fig.2d,d'), *PAGRI* (Fig.2e,e'), and *MAZ* (Fig.2f,f') mRNAs are expressed in the VZ/SVZ
265 and also in cells of the SP/CP. In addition to being expressed in the proliferative zones of the
266 cerebral cortex *KIF22*, *ALDOA*, *HIRIP3*, *PAGRI*, and *MAZ* are also expressed in the ventricular
267 zone of the ganglionic eminences where interneuron progenitors reside suggesting the hypothesis
268 that interneuron development may be affected by alterations in their dosage in the *16p11.2* CNV.



270 **Figure 2: *In situ* hybridisation of candidate genes.** a) PAX6 protein (green) at 12pcw. a-a'*)
271 show high magnification images of PAX6 protein expression in the a') SP/CP, a*) IZ, a'') SVZ
272 and a'*) VZ. Low magnification scale bars = 50µm, high magnification scale bars = 10µm. b)
273 Low magnification image of *KIF22* mRNA in the 12pcw human fetal cortex, b') High
274 magnification showing *KIF22* mRNA (blue) to be predominantly expressed in the germinative
275 zones. c) Low magnification image of *ALDOA* mRNA in the 12pcw human fetal cortex, b') High
276 magnification showing *ALDOA* mRNA (blue) to be predominantly expressed in the germinative
277 zones but also some expression in the IZ and CP. d) Low magnification image of *HIRIP3* mRNA
278 in the 12pcw human fetal cortex, d') High magnification showing *HIRIP3* mRNA (blue) to be
279 expressed throughout the telencephalic wall. e) Low magnification image of *PAGRI* mRNA in
280 the 12pcw human fetal cortex, e') High magnification showing *PAGRI* mRNA (blue) to be
281 expressed throughout the telencephalic wall. f) Low magnification image of *MAZ* mRNA in the
282 12pcw human fetal cortex, f') High magnification showing *MAZ* mRNA (blue) to be expressed
283 throughout the telencephalic wall. For ISH, low magnification scale bars = 2mm and high
284 magnification scale bars = 100µm.

285

286 To conclude, of all the 29 *16p11.2* transcripts, five, *KIF22*, *ALDOA*, *HIRIP3*, *PAGRI*, and *MAZ*,
287 are expressed in the ventricular and subventricular zones at higher levels than in post-mitotic cells.
288 Of these only two, *KIF22* and *ALDOA*, are significantly enriched in progenitors compared to post-
289 mitotic cells making them candidates for having specific roles in neurogenesis in the developing
290 human fetal cerebral cortex. Although both are enriched in progenitors, *KIF22* and *ALDOA*
291 transcript expression shows notable differences: *KIF22* transcripts are more restricted to

292 progenitors and their levels vary as the cell-cycle progresses. We next describe the expression of
293 KIF22 and ALDOA protein over a range of developmental stages.

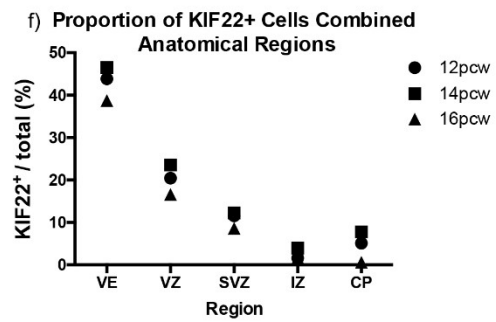
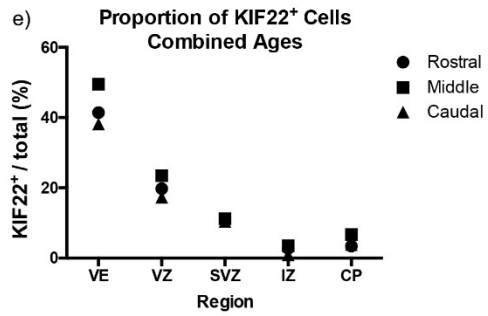
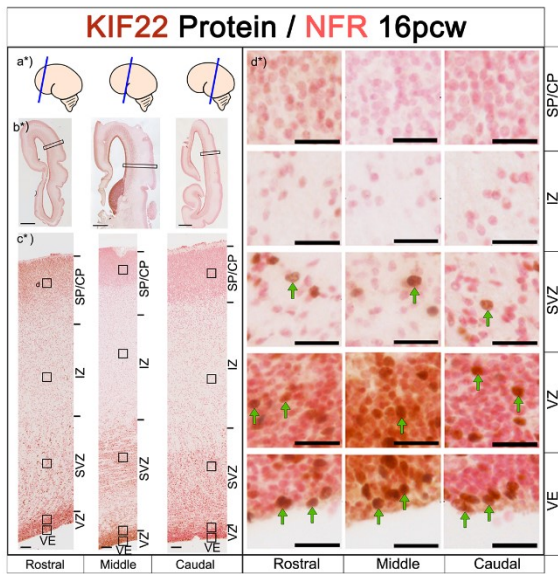
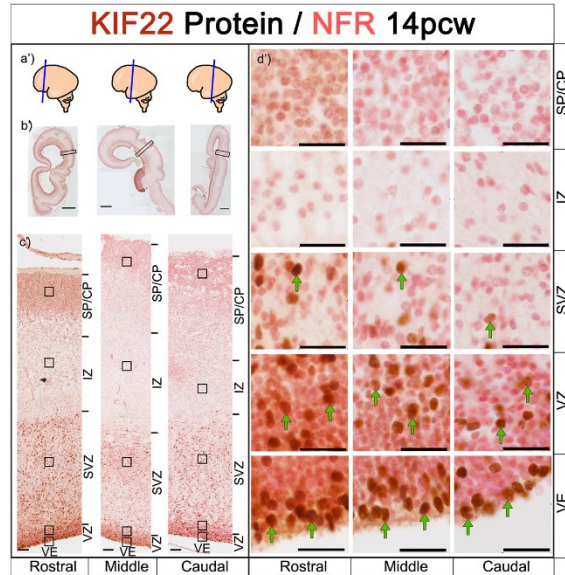
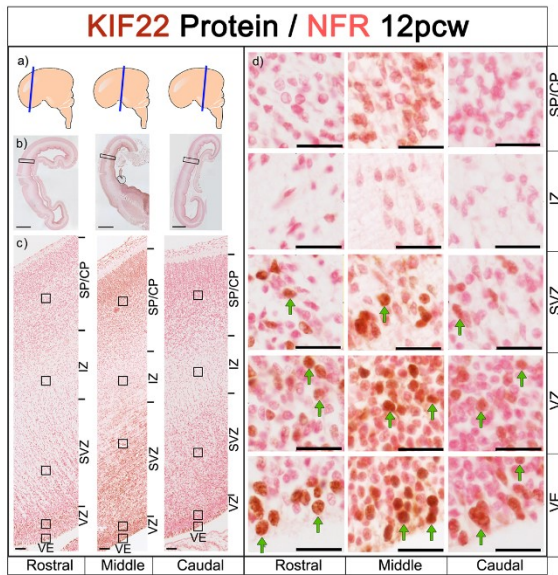
294

295 **KIF22 protein is expressed in germinal zones of 12, 14 and 16 PCW cortex**

296 Here we characterize KIF22 protein expression during human corticogenesis. Coronal cortex
297 sections spaced along the rostral-caudal axis were immunostained for KIF22 protein and
298 counterstained with Nuclear Fast Red (NFR) to show cytoarchitecture. KIF22⁺ (brown) and KIF22⁻
299 (red) cells were counted for each region in the telencephalic wall (VE, VZ, SVZ, IZ and CP) (see
300 methods for details of sampling) and lamination was identified by cell density (Bayer and Altman,
301 2002, 2005). These data are shown for three developmental stages, 12 PCW (Fig.3 a-d), 14 PCW
302 (Fig.3 a'-d'), and 16 PCW (Fig.3 a*-d*). At all stages and rostro-caudal positions KIF22
303 expressing cells appear most abundant in the VE followed by the VZ and SVZ with the IZ and CP
304 presenting a very low to complete absence of KIF22 (Fig.3 c, c', and c* with higher magnification
305 of boxed regions from each zone shown in d, d', and d* respectively, green arrows indicate
306 examples of individual KIF22⁺ cells).

307

308 We next pooled KIF22⁺ cell count data in two ways to compare between all ages (Fig.3e) and
309 anatomical regions (Fig.3f) and found that the percentage of KIF22⁺ cells in the VE (40-50%) was
310 consistently higher than other regions, followed by the VZ (20-30%) and SVZ (10%), with even
311 fewer cells (<10%) in the IZ, and CP (Fig.3e,f). This result describes KIF22 protein as
312 predominantly restricted to a subset of cells in the germinal zones of the developing cortex at all
313 stages studied.

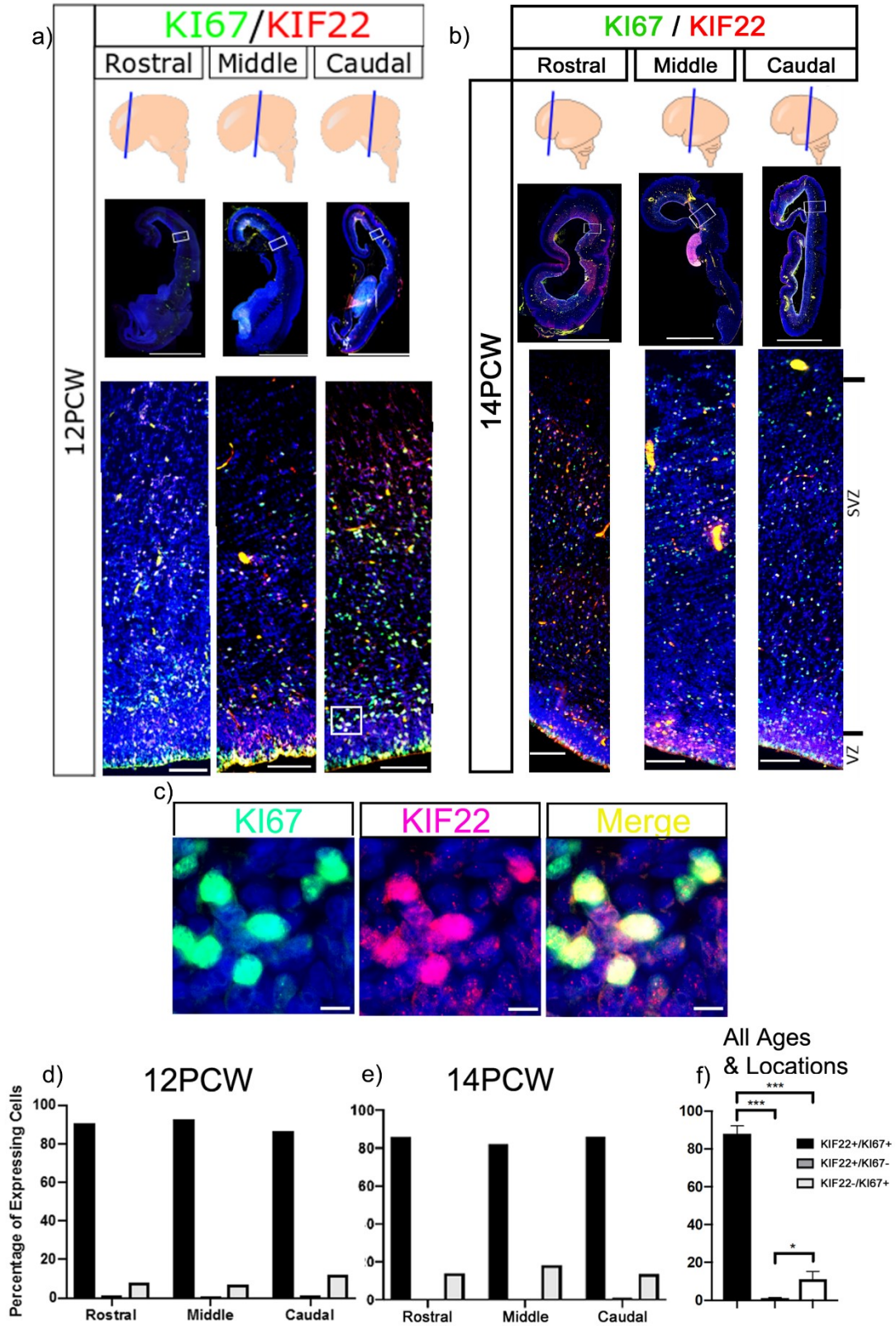


315 **Figure 3: KIF22 protein expression levels in the cerebral cortex at 12, 14 and 16 PCW** a, a',
316 a*) schematic showing brain regions sectioned. b, b', b*) images of whole brain section, scale bars
317 =2mm. c, c', c*) sections spanning the rostral-caudal axis showing KIF22 expression in the
318 telencephalic wall, scale bars = 100µm. d, d', d*) high magnification images of different cortical
319 zones rostral-caudal. KIF22⁺ cells in brown and examples indicated by green arrows, KIF22⁻ cells
320 in pink, scale bars =25 µm. e) Quantification of KIF22 expressing cells with all three ages
321 combined. f) Quantification of KIF22 expressing cells with rostral, middle, caudal values
322 combined.

323

324 **KIF22 protein expression is restricted to proliferating cells**

325 KIF22 protein expression is almost exclusively restricted to a subset of cells in the proliferative
326 regions. From the scRNA-seq data, we expect these to be progenitor cells (Fig.1). To identify these
327 KIF22 positive cells we performed double immunofluorescence for KIF22 and KI67 (a protein
328 expressed in all proliferating cells (Scholzen and Gerdes, 2000; Miller *et al.*, 2018)). KIF22⁺ cells
329 were predominantly located in the VE, VZ and SVZ (Fig.3), therefore these regions were examined
330 for analysis. Low magnification of KI67/KIF22 staining are shown in 12 PCW (Fig.4a) and 14
331 PCW (Fig.4b) with higher magnification showing individual cells in Fig.4c. Cell counts for
332 KIF22⁺/KI67⁺ labelled cells show that the majority (80-90%) of KI67⁺ cells also express KIF22
333 both at 12 (Fig.4d) and 14 PCW (Fig.4e) or across the rostral-caudal axis. Combining the data for
334 anatomical locations and ages revealed significantly more KIF22⁺/KI67⁺ cells than KIF22⁺/KI67⁻
335 and KIF22⁻/KI67⁺ cells (Fig.4f).



337 **Figure 4: Immunofluorescence of KIF22 and KI67 proteins in the cortex.** a) KIF22 and KI67
338 at 12 PCW, low magnification scale bars = 4mm, high magnification scale bars = 100 μ m. b)
339 KIF22 and KI67 at 14 PCW, low magnification scale bars = 4mm, high magnification scale bars
340 = 100 μ m. c) high magnification of KI67/KIF22 expressing cells. Scale bars = 10 μ m. d)
341 Percentage of cells expressing KIF22, KI67 or both at 12 PCW. e) Percentage of cells expressing
342 KIF22, KI67 or both at 14 PCW. f) Combined data of percentage of cells expressing KIF22,
343 KI67 or both.

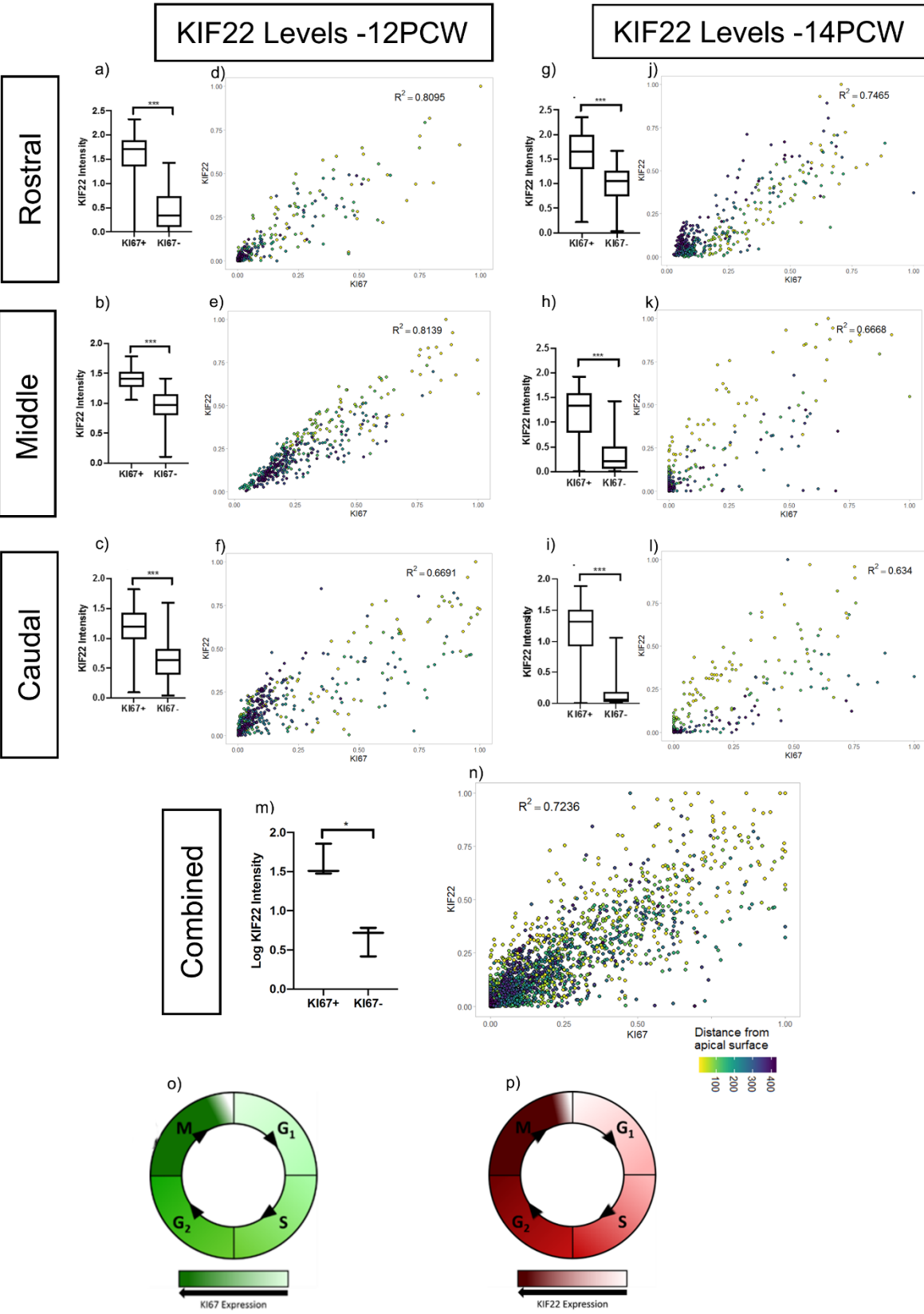
344

345 **KIF22 levels vary with cell-cycle phase**

346 From the scRNA-seq analysis, and the variable KIF22 protein levels in KI67⁺ cells, we
347 hypothesised that KIF22 protein levels change throughout the cell cycle. To test this, we quantified
348 nuclear immunofluorescence intensity of KIF22 and KI67 in two 12 PCW brains (see methods for
349 details of sampling procedure). KI67 protein levels vary during the cell cycle: lowest in G1 phase,
350 increasing through S and G2 to peak in mitosis (Fig.5o) (Scholzen and Gerdes, 2000; Miller *et al.*,
351 2018). We found a strong correlation between KIF22 and KI67 intensity (Brain 1 rostral
352 $R^2=0.8095$, middle $R^2=0.8139$, caudal $R^2= 0.6691$. Brain 2 rostral $R^2 = 0.7489$, middle $R^2=0.7447$,
353 caudal $R^2=0.7763$) (Fig.5d-f). To ensure the correlation observed was not a result of nucleus size
354 changing with cell cycle, we confirmed that KIF22 protein levels did not correlate with nuclear
355 size by DAPI staining (Brain 1 rostral KIF22 $R^2=0.104$, middle KIF22 $R^2=0.0874$, caudal KIF22
356 $R^2=0.2969$. Brain 2 rostral KIF22 $R^2=0.1183$, middle KIF22 $R^2=0.0512$, caudal KIF22
357 $R^2=0.2287$). A strong positive correlation was also observed at 14 PCW (Brain 1 rostral
358 $R^2=0.7465$, middle $R^2=0.6668$, caudal $R^2= 0.634$, Fig.5j-l). Again, we confirmed that KIF22

359 protein levels did not correlate with nuclear size (rostral KIF22 $R^2=0.1239$, middle KIF22
360 $R^2=0.0599$, caudal KIF22 $R^2=0.0229$). This demonstrates that the correlation between KI67 and
361 KIF22 is consistent between ages and rostral-caudal location. Combining all values of KI67/KIF22
362 nuclear intensity values showed that KIF22 was expressed at significantly higher levels in KI67⁺
363 cells (Fig.5m) with a strong correlation ($R^2=0.7236$) between KIF22 and KI67 levels (Fig.5n).
364 Although KIF22 expressing cells were scattered throughout the VE, VZ and SVZ there was a
365 general trend for the cells expressing the highest levels of KIF22 to be closest to the apical surface
366 (yellow coloured dots on scatterplots Fig.5d-f, j-l,n) with lower expressing cells tending to be
367 further from the apical surface (blue coloured dots on scatterplots Fig.5d-g, j-l,n). During
368 interkinetic nuclear movement radial glial cell nuclei move to the apical surface to perform mitosis
369 so this spatial distribution suggests KIF22 is expressed at high levels by radial glial cells
370 undergoing mitosis at the apical surface of the VZ. Cerebral cortex progenitor that do not undergo
371 interkinetic movement (intermediate progenitors and outer sub-ventricular zone progenitors)
372 cannot be assigned to cell cycle phase using their position as we were able to do for radial glial
373 cells which do undergo interkinetic movement. As *KIF22* transcript levels were at highest in all
374 progenitors in M-phase (Fig.1h) we suspect that cells expressing high levels of KIF22 and KI67
375 further away from the apical surface are cortical progenitors in M-phase not undergoing
376 interkinetic movement but further experiments would be needed to show this.

377 From these data we show that, for radial glial cells, KIF22 protein levels change throughout the
378 cell cycle in positive correlation with KI67: KIF22 is present in G1 and increases through S and
379 G2 phase to peak in mitosis (Fig.5p).



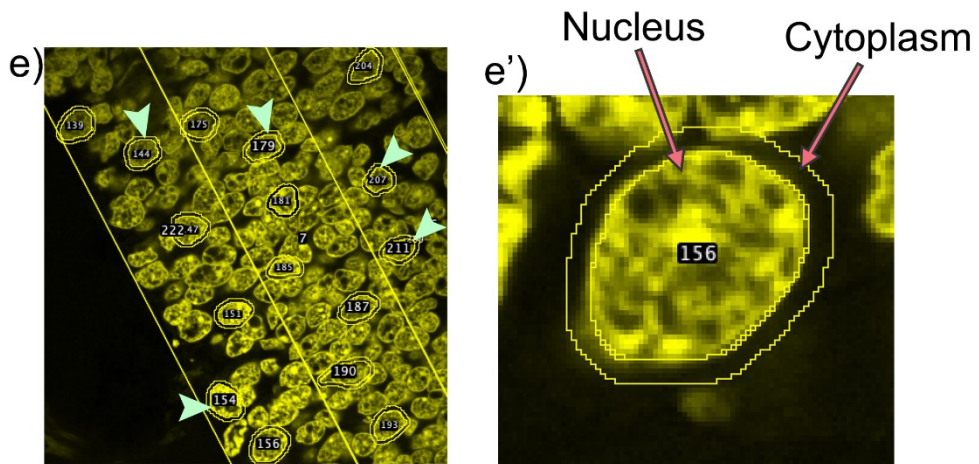
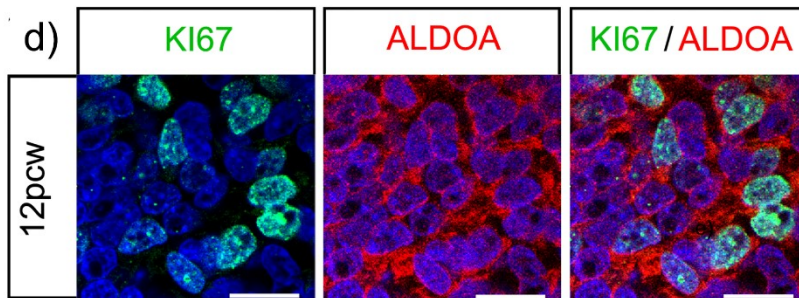
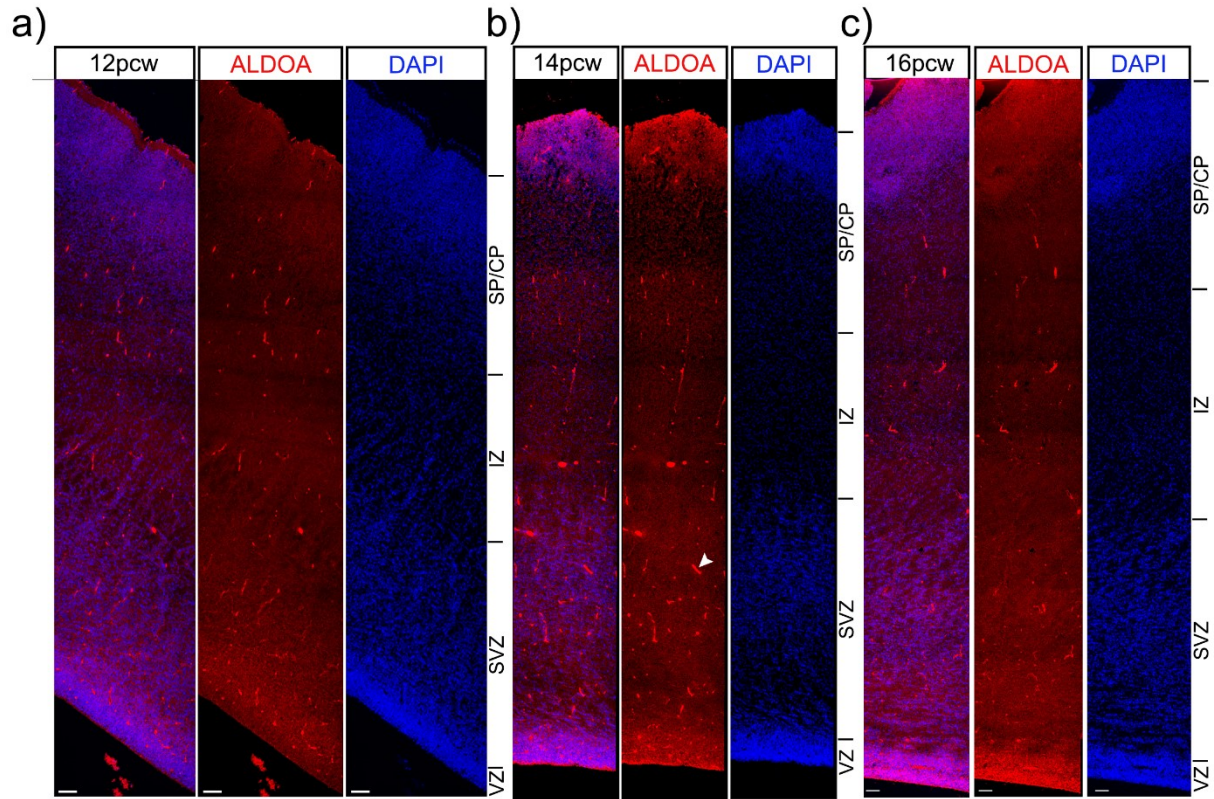
381 **Figure 5: Quantification of KIF22 protein levels.** a,b,c) 12 PCW quantification of KIF22
382 fluorescence intensity in KI67+/KI67- cells (raw data transformation =+1(log), unpaired t-test
383 with Welch's correction, $p < 0.001$). d,e,f) intensity correlations of KIF22 and KI67 nuclear
384 fluorescence intensity at 12 PCW. g, h, i) 14 PCW quantification of KIF22 fluorescence intensity
385 in KI67+/KI67- cells (raw data transformation =+1(log), unpaired t-test with Welch's correction,
386 $p < 0.001$). j, k, l) intensity correlations of KIF22 and KI67 nuclear fluorescence intensity at 14
387 PCW. m) quantification of KIF22 fluorescence intensity in KI67+/KI67- cells 12 and 14 weeks
388 combined (raw data transformation =(log), paired t-test, $p = 0.0122$). n) intensity correlations of
389 KIF22 and KI67 nuclear fluorescence intensity for rostral-caudal points at 12 and 14 PCW with
390 distance from apical surface indicated by dot colour. o) diagram of KI67 protein levels
391 throughout the cell cycle. p) model based on our results of KIF22 protein levels throughout the
392 cell cycle.

393

394 **ALDOA protein is highest in the germinal zones of the cortex**

395 Bioinformatics analysis and *in situ* hybridisation show *ALDOA* mRNA levels decrease as
396 progenitor cells move towards a neuronal fate (Fig.1). Here we used immunofluorescence to
397 characterize *ALDOA* protein expression across the telencephalic wall at 3 developmental time
398 points; at 12, 14 and 16 PCW, *ALDOA* immunofluorescence is most intense in the VZ and SVZ
399 before decreasing in the cortical plate (Fig.6a-c). Double immunofluorescence for KI67 and
400 *ALDOA* viewed at high magnification shows that *ALDOA* protein is primarily localized outside
401 DAPI⁺ nuclei in the cytoplasm and that *ALDOA* is expressed by KI67⁺ progenitor cells and also

402 by cells that do not express KI67 (Fig.6d). The schematic (Fig.6e and 6e') illustrates the areas used
403 for quantification of nuclear and whole cell ALDOA fluorescence presented in Fig.6.



405 **Figure 6: ALDOA protein expression in the cortex.** ALDOA protein expression across the
406 telencephalic wall at a) 12, b) 14 and c) 16 pcw. Scale bars = 100 μ m. White arrow indicates non-
407 specific binding to blood vessels. d) high magnification immunofluorescence of ALDOA and
408 KI67 proteins, scale bar = 10 μ m. e) low power image showing how cells were randomly selected
409 for analysis using the DAPI channel. e') high power image showing how the nucleus and
410 cytoplasm were delineated for analysis

411

412 **ALDOA protein levels do not correlate with proliferation**

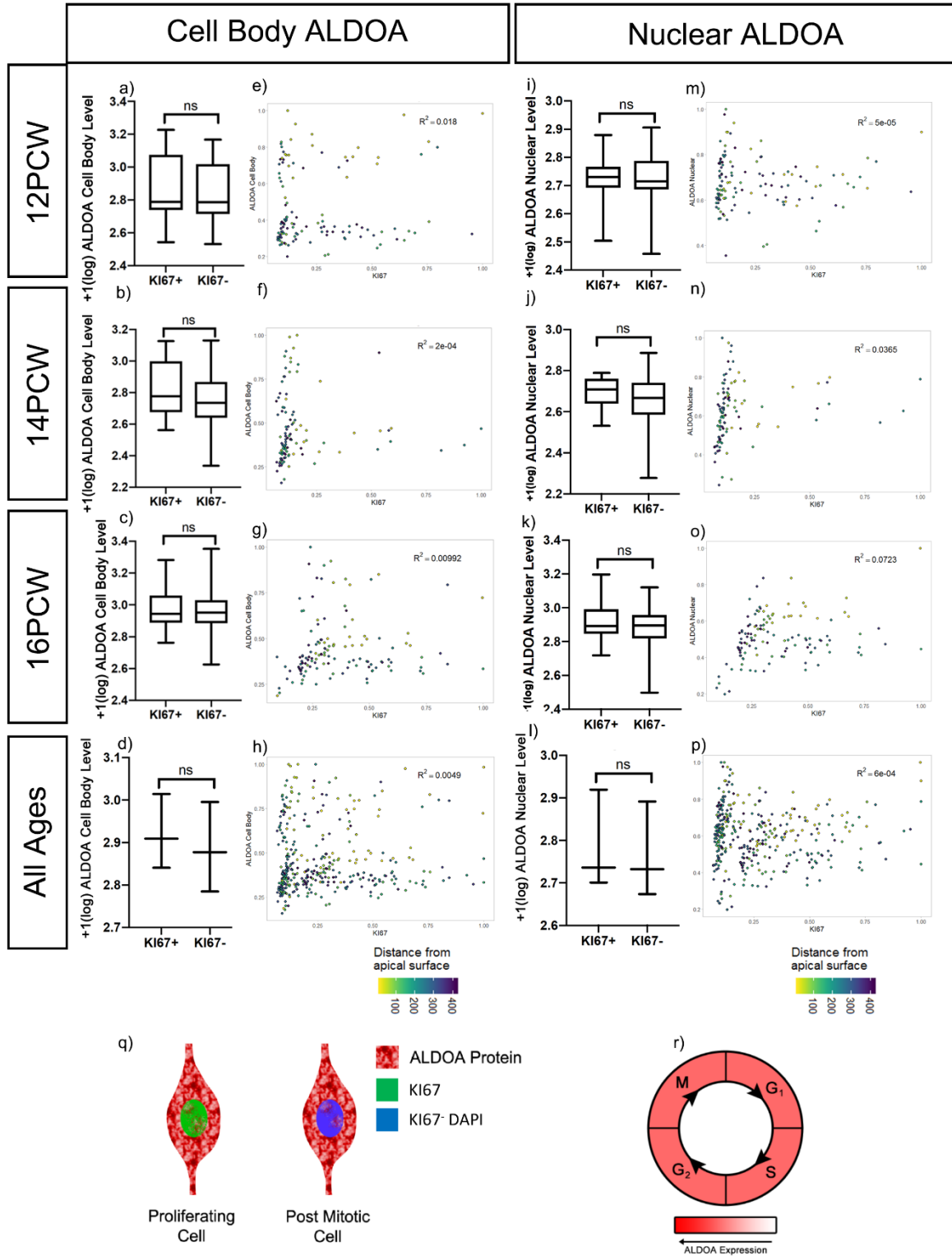
413 Although examination of ALDOA mRNA expression indicated it was enriched in progenitors we
414 were unable to find a significant difference in ALDOA protein levels between KI67⁺ and KI67⁻
415 cells at 12 (Fig.7a), 14 (Fig.7b) and 16 PCW (Fig.7c) in the human cortex. To look for any
416 fluctuation in ALDOA levels with the cell cycle we quantified immunofluorescence for KI67 and
417 cell body ALDOA '(nucleus and adjacent cell body) using the same analysis as that described
418 above for KIF22, and found no correlation or discernible pattern at 12 (Fig.7e) ($R^2= 0.018$), 14
419 (Fig.7f) ($R^2= 2e-4$) or 16 PCW (Fig.7g) ($R^2= 0.00992$). These data show that in human cortex
420 development, cellular ALDOA protein levels do not correlate with proliferation or fluctuate with
421 cell cycle.

422

423 Previous work in different models demonstrated nuclear ALDOA level is greater in proliferating
424 cells (Mamczur, Mazurek and Rakus, 2010; Mamczur *et al.*, 2013). To see if this was the case in
425 human cortex development, we quantified nuclear ALDOA and KI67 (Fig.6e) but found no
426 significant difference in nuclear ALDOA fluorescence between KI67⁺ and KI67⁻ cells at 12

427 (Fig.7i), 14 (Fig.7j) or 16 PCW (Fig.7k). We next tested if nuclear ALDOA levels in proliferating
428 cells varied with cell cycle. Analysis of ALDOA and KI67 nuclear intensity established no
429 correlation or pattern at 12 (Fig.7m) ($R^2= 5e-05$), 14 (Fig.7n) ($R^2= 0.0365$) or 16 PCW (Fig.7o)
430 ($R^2= 0.0723$). This shows nuclear ALDOA levels do not increase with proliferation, nor fluctuate
431 with cell cycle. We combined results across the 12, 14 and 16 PCW. There was no significant
432 difference between KI67⁺ and KI67⁻ cells when examining ALDOA protein intensity in the whole
433 cell (Fig.7d) or the nucleus (Fig.7i). Using the pooled data, there was no correlation or discernible
434 pattern when nuclear ALDOA intensity was graphed against nuclear KI67 level for the whole cell
435 (Fig.7h) ($R^2= 0.0049$) or the nucleus (Fig.7p) ($R^2= 6e-04$).

436



438 **Figure 7: ALDOA protein quantification.** a-d) Cell body ALDOA protein fluorescent intensity
439 in KI67+ and KI67- cells at a) 12 PCW (raw data transformation =+1(log), bimodal distribution,
440 Mann-Whitney test, $p = 0.3702$), b) 14 PCW (raw data transformation =+1(log), normal
441 distribution, unpaired t-test with Welch's correction, $p = 0.2032$), c) 16 PCW (raw data
442 transformation =+1(log), normal distribution, unpaired t-test with Welch's correction, $p =$
443 0.3523). d) ALDOA cell body protein fluorescent intensity in KI67+ and KI67- cells, 12, 14 and
444 16 PCW individual datasets averaged, (raw data transformation =+1(log)), paired t-test, $p =$
445 0.0836 . e-h) ALDOA cellular protein intensity levels is correlated to nuclear KI67 protein
446 intensity at e)12, f)14 and g)16 PCW with distance from ventricular edge indicated. h) ALDOA
447 whole cell protein intensity levels correlated to nuclear KI67 protein intensity pooled 12, 14, 16
448 PCW. i-l) Nuclear ALDOA protein fluorescent intensity in KI67+ and KI67- cells at i) 12 PCW
449 (raw data transformation =+1(log), normal distribution, unpaired t-test with Welch's correction,
450 $p = 0.7543$), j) 14 PCW (raw data transformation =+1(log), normal distribution, unpaired t-test
451 with Welch's correction, $p = 0.0694$), k) 16 PCW (raw data transformation =+1(log), normal
452 distribution, unpaired t-test with Welch's correction, $p = 0.0772$). l) ALDOA nuclear protein
453 fluorescent intensity in KI67+ and KI67- cells, 12, 14 and 16 PCW individual datasets averaged,
454 (raw data transformation =+1(log)), paired t-test, $p = 0.1330$. m-p) ALDOA nuclear protein
455 intensity levels is correlated to nuclear KI67 protein intensity at m)12, n)14 and o)16 PCW with
456 distance from ventricular edge indicated. p) ALDOA nuclear protein intensity levels correlated
457 to nuclear KI67 protein intensity pooled 12, 14, 16 PCW. q) schematic demonstrating ALDOA
458 protein is predominantly in the cytoplasm and lower in the nucleus in both KI67+ proliferating
459 cells and KI67- post mitotic cells. r) model showing ALDOA levels do not change with the cell
460 cycle.

461 **Discussion**

462 ***16p11.2* transcript expression during human neurogenesis.**

463 The *16p11.2* CNV is a polygenic mutation that causes NDDs and the current study identified a
464 number of the 29 *16p11.2* transcripts expressed in progenitor cells of the cerebral cortex. In
465 addition to *ALDOA* and *KIF22* that are significantly enriched in progenitors, several other
466 transcripts (e.g. *HIRIP3*, *PAGRI*, and *MAZ*) are also expressed in progenitors albeit at lower levels
467 and are not significantly down-regulated as cells become post-mitotic. The simultaneous
468 expression of multiple *16p11.2* genes in cells undergoing neurogenesis suggests that these cells
469 may be particularly vulnerable to simultaneous alteration in their dosage as a consequence of the
470 *16p11.2* microdeletion or microduplication. This lends support to the hypothesis that neurogenesis
471 is disrupted in *16p11.2* CNV patients and that this contributes to subsequent development of
472 NDDs.

473 In this study we focused on the expression of *16p11.2* genes in progenitors of the developing
474 cerebral cortex that will give rise to excitatory neurons. However, *KIF22*, *ALDOA*, *HIRIP3*,
475 *PAGRI*, and *MAZ* transcripts are also expressed in the ventricular zone of the ganglionic
476 eminences where the progenitors of the inhibitory interneurons that subsequently migrate into the
477 cerebral cortex reside. Simultaneous increase or decrease of these transcripts in interneuron
478 progenitors resulting from the *16p11.2* CNV may therefore have an impact on the neurogenesis or
479 differentiation of interneurons.

480 **KIF22**

481 KIF22 is a multifunctional protein that can regulate cell proliferation through at least two distinct
482 mechanisms. First, KIF22 is a kinesin-like microtubule-based motor that binds microtubules and

483 chromosomes during mitosis and regulates mitotic spindle microtubule stability and
484 symmetric/asymmetric cell division (Tokai *et al.*, 1996; Tokai-Nishizumi *et al.*, 2005; Sun and
485 Hevner, 2014). Second, KIF22 regulates the expression of the cell-cycle regulator CDC25C.
486 During cell division, CDC25C dephosphorylates CDK1, thus activating the CDK1-cyclinB
487 complex while the CDK1-cyclin B complex phosphorylates CDC25C, causing an amplification
488 loop to drive cells to mitosis (Nilsson and Hoffmann, 2000). KIF22 directly transcriptionally
489 represses CDC25C and inhibits mitosis; this transcriptional repression of CDC25C is dependent
490 on KIF22 being phosphorylated on Thr463 (Ohsugi *et al.*, 2003; Yu *et al.*, 2014). KIF22 depletion
491 in a tumor cell line accelerates the G2/M transition and slows M/G1 transition (Yu *et al.*, 2014).

492 Overall, it therefore appears that KIF22 can act at several different points in the cell cycle making
493 it difficult to predict how increased or decreased dosage of KIF22 in the *16p11.2* microduplication
494 or microdeletion respectively would impact cell cycle in the specific context of cerebral cortex
495 neural progenitors especially in light of the concomitant altered dosage of other *16p11.2* genes co-
496 expressed with *KIF22* in progenitors. Our observation that *KIF22* mRNA and KIF22 protein levels
497 both increase during the cell cycle to achieve highest levels in G2/M phase that drop as cells enter
498 G1 phase implies that KIF22 protein does not persist for long after it is translated and is degraded
499 at the end of M-phase suggesting that both transcriptional and post-transcriptional mechanisms
500 regulate its levels. A clear outcome of our study is that KIF22 levels positively correlate with KI67
501 in neural progenitors and steadily rise as the cell progresses through G1>S>G2>M phases
502 culminating in the maximum level during M-phase. One possibility is that KIF22 is required to
503 reach a threshold for mitosis to occur, after which its levels must decrease sufficiently to allow
504 mitotic exit. Whether cells undertake proliferative or neurogenic divisions is a process heavily
505 controlled by cell cycle length (Borrell and Calegari, 2014). Perturbing *KIF22* gene dosage as a

506 consequence of the *16p11.2* CNV might affect the timing of KIF22 protein reaching this threshold
507 in neural progenitors and therefore affect cell-cycle kinetics and perturb neurogenesis and neuronal
508 output. Our results suggest the hypothesis that KIF22 regulates neurogenesis in the human
509 developing cortex through cell-cycle regulation.

510

511 ALDOA

512 The process of brain development requires a vast and consistent supply of energy. Glucose is the
513 predominant energy substrate for the fetal brain (Gustafsson, 2009), therefore efficient and
514 controlled glycolysis is essential for normal brain development. ALDOA is required for the fourth
515 step of glycolysis, conversion of fructose 1,6-biphospate to dihydroxyacetone phosphate and
516 gluteraldehyde 3-phosphate. The metabolic role of cytoplasmic ALDOA is well established, and
517 ALDOA also has other non-glycolytic “moonlighting” roles such as regulating mitochondrial
518 function and cytoskeleton stability (Orosz, Christova and Ovadi, 1988; Pagliaro and Taylor, 1992;
519 Kao *et al.*, 1999; Jewett and Sibley, 2003; Buscaglia *et al.*, 2006). In addition to its cytoplasmic
520 roles, ALDOA has been observed in the nucleus (Mamczur and Dzugaj, 2008; Mamczur, Mazurek
521 and Rakus, 2010; Mamczur *et al.*, 2013) where it has been suggested to impact cell cycle by
522 positively regulating cyclin D1 expression to mediate G1/S progression (Ritterson Lew and Tolan,
523 2012; Fu *et al.*, 2018). Cell-culture studies show ALDOA sub-cellular localisation depends on the
524 availability of energetic substrates, with addition of glucose driving ALDOA protein to the
525 cytoplasm (Mamczur *et al.*, 2013). Therefore, it is likely the primary role for ALDOA is metabolic
526 when cells require, and have available to them, large amounts of energy. The majority of ALDOA
527 studies have used highly abnormal cancer tissue, or artificial cell culture systems in which

528 glycolytic enzymes have been shown to be increased (Ritterson Lew and Tolan, 2012; Mamczur
529 *et al.*, 2013; Fu *et al.*, 2018; Pollen *et al.*, 2019). How these observations of ALDOA in a variety
530 of systems relate to its role in human cerebral cortex development is unclear.

531 Altering ALDOA dosage in the developing brain will likely impact energy metabolism by altering
532 the flow of metabolites through the glycolytic pathway and impacting subsequent pathways which
533 feed on outputs of glycolysis. Disruption to energy metabolism during development has previously
534 been linked to ASD and ADHD (Rash *et al.*, 2018). The offspring of hyperglycemic mice presented
535 microcephaly, a phenocopy of the microcephaly observed in *16p11.2* microduplication patients
536 (Rash *et al.*, 2018) and disruptions to energy metabolism may contribute to the microcephaly seen
537 in the offspring of Zika infected mothers (Gilbert-Jaramillo *et al.*, 2019). No homozygous null
538 ALDOA patients have been identified suggesting it is essential for life, but patients with changes
539 to ALDOA levels have been identified; one patient with reduced ALDOA activity presented
540 microcephaly (Kreuder *et al.*, 1996) and another presented intellectual disability (Beutler *et al.*,
541 1973). Of particular interest is the finding of schizophrenia patients with upregulated cortical
542 ALDOA levels (Beasley *et al.*, 2006) and *16p11.2* microduplication is strongly associated with
543 risk of schizophrenia. This information, coupled with our results that ALDOA is expressed in all
544 cell types, make it clear that any changes to ALDOA dose will perturb energy metabolism at many
545 stages in the brain, impacting its development.

546 ALDOA is much more abundant in the cytoplasm and we also found no clear relationship between
547 cell body ALDOA levels and cell proliferation status. Nuclear ALDOA has been linked to cell
548 proliferation (Mamczur, Mazurek and Rakus, 2010; Mamczur *et al.*, 2013; Fu *et al.*, 2018) but we
549 found no clear relationship between nuclear ALDOA protein levels and cell proliferation status.
550 While *ALDOA* mRNA levels are higher in proliferating cells compared to non-proliferating cells,

551 quantitative analysis of ALDOA protein revealed that ALDOA protein persists once cells exit
552 mitosis. Therefore, while ALDOA protein is abundant in progenitor cells of the developing human
553 cerebral cortex and so may play a role in neurogenesis phenotypes, the persistent expression of
554 ALDOA protein as cells become post-mitotic argues against a specific role in neurogenesis and
555 raises the additional possibility that ALDOA also plays roles in differentiated neurons.

556

557 **Conclusion**

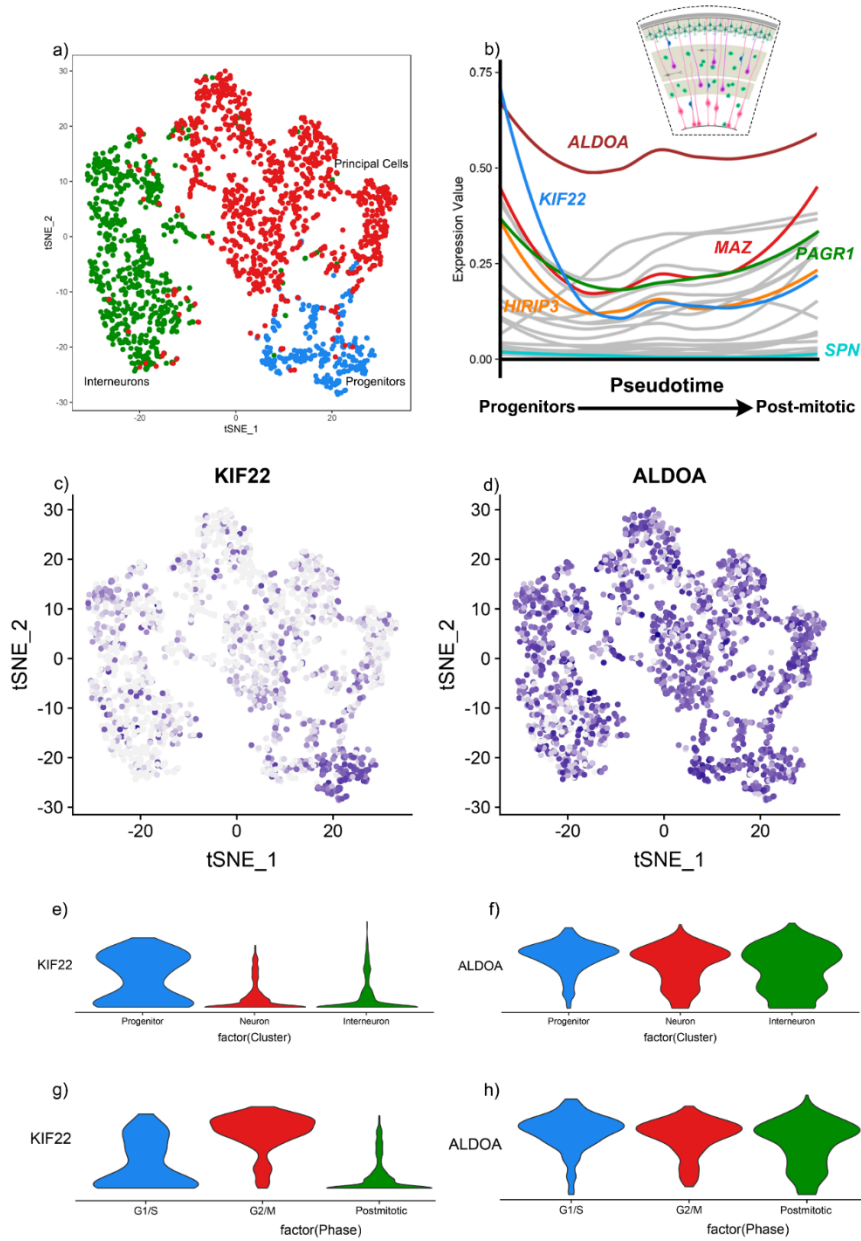
558 Our study of *16p11.2* gene expression in developing human fetal cerebral cortex indicates that
559 altered dosage of *KIF22*, *ALDOA*, *HIRIP3*, *PAGR1*, and *MAZ* caused by the *16p11.2*
560 microduplication or microdeletion may impact on neurogenesis in the developing human cortex
561 and we identified *KIF22* being a strong candidate for having a specific role in neurogenesis.
562 Further studies are required to unpick the mechanisms involved, but given the nature of the tissue,
563 the scope for studying this *in vivo* is currently limited. However, growth of new model systems in
564 which *16p11.2* gene expression can be manipulated such as human cerebral organoids will provide
565 the opportunity address these questions.

566

567 **Acknowledgements**

568 This work was funded by BBSRC grant (BB/M00693X/1) and the Simons Initiative for the
569 Developing Brain (SFARI - 529085). SM was supported by a BBSRC EASTBIO PhD studentship.
570 The human embryonic and fetal material was provided by the Joint MRC / Wellcome
571 (MR/R006237/1) Human Developmental Biology Resource (www.hdbr.org).

572 We thank Katherine Howe for her assistance with designing *in situ* probes and undergraduate
 573 student Emma Fowler (EF funded by a WR Henderson Scholarship) for her assistance with
 574 quantification



575

576 **Supplementary Figure 1: Bioinformatics analysis of Zhong et al scRNA-seq dataset which**
577 **included all regions of the telencephalic wall in samples from 8-36GW. a) tSNE clustering of**
578 **cell types. b) changing mRNA expression levels of 16p11.2 genes as cells move from**
579 **progenitors to neurons. Schematic of human cortex with dotted box indicates that all the regions**
580 **of the cortex were used in this dataset. c) *KIF22* gradient plot. d) *ALDOA* gradient plot. e) Violin**
581 **plots showing distribution of *KIF22* in different cell types. f) Violin plots showing distribution of**
582 ***ALDOA* in different cell types. g) Violin plots showing distribution of *KIF22* at different cell**
583 **cycle stages. h) Violin plots showing distribution of *ALDOA* at different cell cycle stages.**

584

585

586

587

588

589

590

591

592

593

594

595

596 **References**

- 597 Bayer SA, Altman J. 2002. *The Human Brain During the Late First Trimester*. Taylor & Francis
598 Group.
- 599 Bayer SA, Altman J. 2005. *The Human Brain During The Second Trimester*. CRC Press Taylor
600 & Francis Group.
- 601 Beasley CL, Pennington K, Behan A, Wait R, Dunn MJ, Cotter D. 2006. Proteomic analysis of
602 the anterior cingulate cortex in the major psychiatric disorders: Evidence for disease-
603 associated changes. *Proteomics*. 6:3414–3425.
- 604 Beutler E, Scott S, Bishop A, Margolis N, Matsumoto F, Kuhl W. 1973. Red cell aldolase
605 deficiency and hemolytic anemia: a new syndrome. *Trans Assoc Am Physicians*. 86:154–
606 166.
- 607 Bijlsma EK, Gijsbers AC, Schuurs-Hoeijmakers JH, van Haeringen A, Fransen van de Putte DE,
608 Anderlid BM, Lundin J, Lapunzina P, Perez Jurado LA, Delle Chiaie B, Loeys B, Menten
609 B, Oostra A, Verhelst H, Amor DJ, Bruno DL, van Essen AJ, Hordijk R, Sikkema-Raddatz
610 B, Verbruggen KT, Jongmans MC, Pfundt R, Reeser HM, Breuning MH, Ruivenkamp CA.
611 2009. Extending the phenotype of recurrent rearrangements of 16p11.2: deletions in
612 mentally retarded patients without autism and in normal individuals. *Eur J Med Genet*.
613 52:77–87.
- 614 Blackmon K, Thesen T, Green S, Ben-Avi E, Wang X, Fuchs B, Kuzniecky R, Devinsky O.
615 2018. Focal Cortical Anomalies and Language Impairment in 16p11.2 Deletion and
616 Duplication Syndrome. *Cereb Cortex*. 28:2422–2430.

617 Blaker-Lee A, Gupta S, McCammon JM, De Rienzo G, Sive H. 2012. Zebrafish homologs of
618 genes within 16p11.2, a genomic region associated with brain disorders, are active during
619 brain development, and include two deletion dosage sensor genes. *Dis Model Mech.* 5:834–
620 851.

621 Blumenthal I, Ragavendran A, Erdin S, Klei L, Sugathan A, Guide JR, Manavalan P, Zhou JQ,
622 Wheeler VC, Levin JZ, Ernst C, Roeder K, Devlin B, Gusella JF, Talkowski ME. 2014.
623 Transcriptional consequences of 16p11.2 deletion and duplication in mouse cortex and
624 multiplex autism families. *Am J Hum Genet.* 94:870–883.

625 Borrell V, Calegari F. 2014. Mechanisms of brain evolution: regulation of neural progenitor cell
626 diversity and cell cycle length. *Neurosci Res.* 86:14–24.

627 Budday S, Steinmann P, Ellen K. 2015. Physical biology of human brain development. *Frontiers*
628 *in Cellular Neuroscience* 9:257

629 Buscaglia CA, Penesetti D, Tao M, Nussenzweig V. 2006. Characterization of an aldolase-
630 binding site in the Wiskott-Aldrich syndrome protein. *J Biol Chem.* 281:1324–1331.

631 Bystron, I., Blakemore, C. and Rakic, P. 2008. Development of the human cerebral cortex:
632 Boulder Committee revisited. *Nat Rev Neurosci* 9, 110-122.

633 Clowry, G., Molnar, Z. and Rakic, P. (2010). Renewed focus on the developing human
634 neocortex. *J Anat* 217, 276-288.

635 de Anda FC, Rosario AL, Durak O, Tran T, Graff J, Meletis K, Rei D, Soda T, Madabhushi R,
636 Ginty DD, Kolodkin AL, Tsai LH. 2012. Autism spectrum disorder susceptibility gene
637 TAOK2 affects basal dendrite formation in the neocortex. *Nat Neurosci.* 15:1022–1031.

638 Escamilla, C. O., Filonova, I., Walker, A. K., Xuan, Z. X., Holehonnur, R., Espinosa, F., Liu, S.,
639 Thyme, S. B., Lopez-Garcia, I. A., Mendoza, D. B., et al. (2017). Kctd13 deletion
640 reduces synaptic transmission via increased RhoA. *Nature* 551, 227-231.

641

642 Fu H, Gao H, Qi X, Zhao L, Wu D, Bai Y, Li H, Liu X, Hu J, Shao S. 2018. Aldolase A
643 promotes proliferation and G1/S transition via the EGFR/MAPK pathway in non-small cell
644 lung cancer. *Cancer Commun.* 38:18.

645 Gilbert-Jaramillo J, Garcez P, James W, Molnár Z, Clarke K. 2019. The potential contribution of
646 impaired brain glucose metabolism to congenital Zika syndrome. *J Anat.* 235:468-480.

647 Girirajan S, Eichler EE. 2010. Phenotypic variability and genetic susceptibility to genomic
648 disorders. *Hum Mol Genet.* 19:R176–R187.

649 Golzio C, Willer J, Talkowski ME, Oh EC, Taniguchi Y, Jacquemont S, Reymond A, Sun M,
650 Sawa A, Gusella JF, Kamiya A, Beckmann JS, Katsanis N. 2012. KCTD13 is a major driver
651 of mirrored neuroanatomical phenotypes of the 16p11.2 copy number variant. *Nature.*
652 485:363–367.

653 Gustafsson J. 2009. Neonatal energy substrate production. *Indian J Med Res.* 130:618–623.

654 Horev G, Ellegood J, Lerch JP, Son YE, Muthuswamy L, Vogel H, Krieger AM, Buja A,
655 Henkelman RM, Wigler M, Mills AA. 2011. Dosage-dependent phenotypes in models of
656 16p11.2 lesions found in autism. *Proc Natl Acad Sci U S A.* 108:17076–17081.

657 Jewett TJ, Sibley LD. 2003. Aldolase forms a bridge between cell surface adhesins and the actin
658 cytoskeleton in apicomplexan parasites. *Mol Cell.* 11:885–894.

659 Kao AW, Noda Y, Johnson JH, Pessin JE, Saltiel AR. 1999. Aldolase mediates the association of
660 F-actin with the insulin-responsive glucose transporter GLUT4. *J Biol Chem.* 274:17742–
661 17747.

662 Kreuder J, Borkhardt A, Repp R, Pekrun A, Göttische B, Gottschalk U, Reichmann H,
663 Schachenmayr W, Schlegel K, Lampert F. 1996. Brief report: inherited metabolic myopathy
664 and hemolysis due to a mutation in aldolase A. *N Engl J Med.* 334:1100–1104.

665 Kumar RA, KaraMohamed S, Sudi J, Conrad DF, Brune C, Badner JA, Gilliam TC, Nowak NJ,
666 Cook EH Jr, Dobyns WB, Christian SL. 2008. Recurrent 16p11.2 microdeletions in autism.
667 *Hum Mol Genet.* 17:628–638.

668 Levy D, Ronemus M, Yamrom B, Lee YH, Leotta A, Kendall J, Marks S, Lakshmi B, Pai D, Ye
669 K, Buja A, Krieger A, Yoon S, Troge J, Rodgers L, Iossifov I, Wigler M. 2011. Rare de
670 novo and transmitted copy-number variation in autistic spectrum disorders. *Neuron.*
671 70:886–897.

672 Ma T, Wang C, Wang L, Zhou X, Tian M, Zhang Q, Zhang Y, Li J, Liu Z, Cai Y, Liu F, You Y,
673 Chen C, Campbell K, Song H, Ma L, Rubenstein JL, Yang Z. 2013. Subcortical origins
674 of human and monkey neocortical interneurons. *Nat Neurosci.* 16:1588-97.

675 Macosko EZ, Basu A, Satija R, Nemes J, Shekhar K, Goldman M, Tirosh I, Bialas AR,
676 Kamitaki N, Martersteck EM, Trombetta JJ, Weitz DA, Sanes JR, Shalek AK, Regev A,
677 McCarroll SA. 2015. Highly Parallel Genome-wide Expression Profiling of Individual Cells
678 Using Nanoliter Droplets. *Cell.* 161:1202–1214.

679 Malhotra D, Sebat J. 2012. CNVs: harbingers of a rare variant revolution in psychiatric genetics.
680 *Cell.* 148:1223–1241.

681 Mamczur P, Dzugaj A. 2008. Aldolase A is present in smooth muscle cell nuclei. *Acta Biochim*
682 *Pol.* 55:799–805.

683 Mamczur P, Gamian A, Kolodziej J, Dziegiel P, Rakus D. 2013. Nuclear localization of aldolase
684 A correlates with cell proliferation. *Biochim Biophys Acta.* 1833:2812–2822.

685 Mamczur P, Mazurek J, Rakus D. 2010. Ubiquitous presence of gluconeogenic regulatory
686 enzyme, fructose-1,6-bisphosphatase, within layers of rat retina. *Cell Tissue Res.* 341:213–
687 221.

688 McCarthy SE, Makarov V, Kirov G, Addington AM, McClellan J, Yoon S, Perkins DO, Dickel
689 DE, Kusenda M, Krastoshevsky O, Krause V, Kumar RA, Grozeva D, Malhotra D, Walsh
690 T, Zackai EH, Kaplan P, Ganesh J, Krantz ID, Spinner NB, Roccanova P, Bhandari A,
691 Pavon K, Lakshmi B, Leotta A, Kendall J, Lee Y-H, Vacic V, Gary S, Iakoucheva LM,
692 Crow TJ, Christian SL, Lieberman JA, Stroup TS, Lehtimäki T, Puura K, Haldeman-Englert
693 C, Pearl J, Goodell M, Willour VL, Derosse P, Steele J, Kassem L, Wolff J, Chitkara N,
694 McMahon FJ, Malhotra AK, Potash JB, Schulze TG, Nöthen MM, Cichon S, Rietschel M,
695 Leibenluft E, Kustanovich V, Lajonchere CM, Sutcliffe JS, Skuse D, Gill M, Gallagher L,
696 Mendell NR, Wellcome Trust Case Control Consortium, Craddock N, Owen MJ,
697 O'Donovan MC, Shaikh TH, Susser E, Delisi LE, Sullivan PF, Deutsch CK, Rapoport J,
698 Levy DL, King M-C, Sebat J. 2009. Microduplications of 16p11.2 are associated with
699 schizophrenia. *Nat Genet.* 41:1223–1227.

700 Miller I, Min M, Yang C, Tian C, Gookin S, Carter D, Spencer SL. 2018. Ki67 is a Graded
701 Rather than a Binary Marker of Proliferation versus Quiescence. *Cell Rep.* 24:1105–1112..

702 Nilsson I, Hoffmann I. 2000. Cell cycle regulation by the Cdc25 phosphatase family. *Prog Cell*

703 Cycle Res. 4:107–114.

704 Nuttle X, Giannuzzi G, Duyzend MH, Schraiber JG, Narvaiza I, Sudmant PH, Penn O, Chiatante
705 G, Malig M, Huddleston J, Benner C, Camponeschi F, Ciofi-Baffoni S, Stessman HAF,
706 Marchetto MCN, Denman L, Harshman L, Baker C, Raja A, Penewit K, Janke N, Tang WJ,
707 Ventura M, Banci L, Antonacci F, Akey JM, Amemiya CT, Gage FH, Reymond A, Eichler
708 EE. 2016. Emergence of a Homo sapiens-specific gene family and chromosome 16p11.2
709 CNV susceptibility. *Nature*. 536:205–209.

710 Ohsugi M, Tokai-Nishizumi N, Shiroguchi K, Toyoshima YY, Inoue J, Yamamoto T. 2003.
711 Cdc2-mediated phosphorylation of Kid controls its distribution to spindle and
712 chromosomes. *EMBO J*. 22:2091–2103.

713 Orosz F, Christova TY, Ovádi J. 1988. Modulation of phosphofructokinase action by
714 macromolecular interactions. Quantitative analysis of the phosphofructokinase-aldolase-
715 calmodulin system. *Biochim Biophys Acta*. 957:293–300.

716 Pagliaro L, Taylor DL. 1992. 2-Deoxyglucose and cytochalasin D modulate aldolase mobility in
717 living 3T3 cells. *J Cell Biol*. 118:859–863.

718 Pollen AA, Bhaduri A, Andrews MG, Nowakowski TJ, Meyerson OS, Mostajo-Radji MA, Di
719 Lullo E, Alvarado B, Bedolli M, Dougherty ML, Fiddes IT, Kronenberg ZN, Shuga J,
720 Leyrat AA, West JA, Bershteyn M, Lowe CB, Pavlovic BJ, Salama SR, Haussler D, Eichler
721 EE, Kriegstein AR. 2019. Establishing Cerebral Organoids as Models of Human-Specific
722 Brain Evolution. *Cell*. 176:743–756..

723 Pollen AA, Nowakowski TJ, Chen J, Retallack H, Sandoval-Espinosa C, Nicholas CR, Shuga J,
724 Liu SJ, Oldham MC, Diaz A, Lim DA, Leyrat AA, West JA, Kriegstein AR. 2015.

725 Molecular identity of human outer radial glia during cortical development. *Cell*. 163:55–67.

726 Preibisch S, Saalfeld S, Tomancak P. 2009. Globally optimal stitching of tiled 3D microscopic
727 image acquisitions. *Bioinformatics*. 25:1463–1465.

728 Pucilowska J, Vithayathil J, Pagani M, Kelly C, Karlo JC, Robol C, Morella I, Gozzi A,
729 Brambilla R, Landreth GE. 2018. Pharmacological Inhibition of ERK Signaling Rescues
730 Pathophysiology and Behavioral Phenotype Associated with 16p11.2 Chromosomal
731 Deletion in Mice. *J Neurosci*. 38:6640–6652.

732 Pucilowska J, Vithayathil J, Tavares EJ, Kelly C, Karlo JC, Landreth GE. 2015. The 16p11.2
733 deletion mouse model of autism exhibits altered cortical progenitor proliferation and brain
734 cytoarchitecture linked to the ERK MAPK pathway. *J Neurosci*. 35:3190–3200.

735 Qiu X, Hill A, Packer J, Lin D, Ma Y-A, Trapnell C. 2017. Single-cell mRNA quantification and
736 differential analysis with Census. *Nat Methods*. 14:309–315.

737 Qureshi AY, Mueller S, Snyder AZ, Mukherjee P, Berman JI, Roberts TP, Nagarajan SS, Spiro
738 JE, Chung WK, Sherr EH, Buckner RL. 2014. Opposing brain differences in 16p11.2
739 deletion and duplication carriers. *J Neurosci*. 34:11199–11211.

740 Radonjić NV, Ortega JA, Memi F, Dionne K, Jakovcevski I, Zecevic N. 2014. The complexity of
741 the calretinin-expressing progenitors in the human cerebral cortex. *Front Neuroanat*. 8:82.

742 Rash BG, Micali N, Huttner AJ, Morozov YM, Horvath TL, Rakic P. 2018. Metabolic regulation
743 and glucose sensitivity of cortical radial glial cells. *Proc Natl Acad Sci U S A*. 115:10142–
744 10147.

745 Richter M, Murtaza N, Scharrenberg R, White SH, Johanns O, Walker S, Yuen RKC, Schwanke

746 B, Bedürftig B, Henis M, Scharf S, Kraus V, Dörk R, Hellmann J, Lindenmaier Z, Ellegood
747 J, Hartung H, Kwan V, Sedlacik J, Fiehler J, Schweizer M, Lerch JP, Hanganu-Opatz IL,
748 Morellini F, Scherer SW, Singh KK, Calderon de Anda F. Altered TAOK2 activity causes
749 autism-related neurodevelopmental and cognitive abnormalities through RhoA signaling.
750 2019. *Mol Psychiatry*. 24:1329-1350.

751 Ritterson Lew C, Tolan DR. 2012. Targeting of several glycolytic enzymes using RNA
752 interference reveals aldolase affects cancer cell proliferation through a non-glycolytic
753 mechanism. *J Biol Chem*. 287:42554–42563.

754 Rosenfeld JA, Coppinger J, Bejjani BA, Girirajan S, Eichler EE, Shaffer LG, Ballif BC. 2010.
755 Speech delays and behavioral problems are the predominant features in individuals with
756 developmental delays and 16p11.2 microdeletions and microduplications. *J Neurodev*
757 *Disord*. 2:26–38.

758 Sanders SJ, Ercan-Sencicek AG, Hus V, Luo R, Murtha MT, Moreno-De-Luca D, Chu SH,
759 Moreau MP, Gupta AR, Thomson SA, Mason CE, Bilguvar K, Celestino-Soper PB, Choi
760 M, Crawford EL, Davis L, Wright NR, Dhodapkar RM, DiCola M, DiLullo NM, Fernandez
761 TV, Fielding-Singh V, Fishman DO, Frahm S, Garagaloyan R, Goh GS, Kammela S, Klei
762 L, Lowe JK, Lund SC, McGrew AD, Meyer KA, Moffat WJ, Murdoch JD, O’Roak BJ,
763 Ober GT, Pottenger RS, Raubeson MJ, Song Y, Wang Q, Yaspan BL, Yu TW, Yurkiewicz
764 IR, Beaudet AL, Cantor RM, Curland M, Grice DE, Gunel M, Lifton RP, Mane SM, Martin
765 DM, Shaw CA, Sheldon M, Tischfield JA, Walsh CA, Morrow EM, Ledbetter DH,
766 Fombonne E, Lord C, Martin CL, Brooks AI, Sutcliffe JS, Cook EH Jr, Geschwind D,
767 Roeder K, Devlin B, State, M. W. 2011. Multiple recurrent de novo CNVs, including

768 duplications of the 7q11.23 Williams syndrome region, are strongly associated with autism.
769 *Neuron*. 70:863–885.

770 Scholzen T, Gerdes J. 2000. The Ki-67 protein: from the known and the unknown. *J Cell*
771 *Physiol*. 182:311–322.

772 Shinawi M, Liu P, Kang SH, Shen J, Belmont JW, Scott DA, Probst FJ, Craigen WJ, Graham
773 BH, Pursley A, Clark G, Lee J, Proud M, Stocco A, Rodriguez DL, Kozel BA, Sparagana S,
774 Roeder ER, McGrew SG, Kurczynski TW, Allison LJ, Amato S, Savage S, Patel A,
775 Stankiewicz P, Beaudet AL, Cheung SW, Lupski JR. 2010. Recurrent reciprocal 16p11.2
776 rearrangements associated with global developmental delay, behavioural problems,
777 dysmorphism, epilepsy, and abnormal head size. *J Med Genet*. 47:332–341.

778 Sun T, Hevner RF. 2014. Growth and folding of the mammalian cerebral cortex: from molecules
779 to malformations. *Nat Rev Neurosci*. 15:217–232.

780 Tai DJC, Ragavendran A, Manavalan P, Stortchevoi A, Seabra CM, Erdin S, Collins RL,
781 Blumenthal I, Chen X, Shen Y, Sahin M, Zhang C, Lee C, Gusella JF, Talkowski ME.
782 2016. Engineering microdeletions and microduplications by targeting segmental
783 duplications with CRISPR. *Nat Neurosci*. 19:517–522.

784 Tirosh I, Izar B, Prakadan SM, Wadsworth MH 2nd, Treacy D, Trombetta JJ, Rotem A, Rodman
785 C, Lian C, Murphy G, Fallahi-Sichani M, Dutton-Regester K, Lin J-R, Cohen O, Shah P, Lu
786 D, Genshaft AS, Hughes TK, Ziegler CGK, Kazer SW, Gaillard A, Kolb KE, Villani A-C,
787 Johannessen CM, Andreev AY, Van Allen EM, Bertagnolli M, Sorger PK, Sullivan RJ,
788 Flaherty KT, Frederick DT, Jané-Valbuena J, Yoon CH, Rozenblatt-Rosen O, Shalek AK,
789 Regev A, Garraway LA. 2016. Dissecting the multicellular ecosystem of metastatic

790 melanoma by single-cell RNA-seq. *Science*. 352:189–196.

791 Tokai N, Fujimoto-Nishiyama A, Toyoshima Y, Yonemura S, Tsukita S, Inoue J, Yamamota T.
792 1996. Kid, a novel kinesin-like DNA binding protein, is localized to chromosomes and the
793 mitotic spindle. *EMBO J*. 15:457–467.

794 Tokai-Nishizumi N, Ohsugi M, Suzuki E, Yamamoto T. 2005. The chromokinesin Kid is
795 required for maintenance of proper metaphase spindle size. *Mol Biol Cell*. 16:5455–5463.

796 Trapnell C, Cacchiarelli D, Grimsby J, Pokharel P, Li S, Morse M, Lennon NJ, Livak KJ,
797 Mikkelsen TS, Rinn JL. 2014. The dynamics and regulators of cell fate decisions are
798 revealed by pseudotemporal ordering of single cells. *Nat Biotechnol*. 32:381–386.

799 Ultanir, S. K., Yadav, S., Hertz, N. T., Oses-Prieto, J. A., Claxton, S., Burlingame, A. L., Shokat,
800 K. M., Jan, L. Y. and Jan, Y. N. (2014). MST3 kinase phosphorylates TAO1/2 to enable
801 Myosin Va function in promoting spine synapse development. *Neuron* 84, 968-982.

802 Weiss LA, Shen Y, Korn JM, Arking DE, Miller DT, Fossdal R, Saemundsen E, Stefansson H,
803 Ferreira MA, Green T, Platt OS, Ruderfer DM, Walsh CA, Altshuler D, Chakravarti A,
804 Tanzi RE, Stefansson K, Santangelo SL, Gusella JF, Sklar P, Wu BL, Daly MJ. 2008.
805 Association between microdeletion and microduplication at 16p11.2 and autism. *N Engl J*
806 *Med*. 358:667–675.

807 Yadav, S., Oses-Prieto, J. A., Peters, C. J., Zhou, J., Pleasure, S. J., Burlingame, A. L., Jan, L. Y.
808 and Jan, Y. N. (2017). TAOK2 Kinase Mediates PSD95 Stability and Dendritic Spine
809 Maturation through Septin7 Phosphorylation. *Neuron* 93, 379-393

810 Yu Y, Wang XY, Sun L, Wang YL, Wan YF, Li XQ, Feng YM. 2014. Inhibition of KIF22
811 suppresses cancer cell proliferation by delaying mitotic exit through upregulating CDC25C

812 expression. *Carcinogenesis*. 35:1416–1425.

813 Zhong, S., Zhang, S., Fan, X., Wu, Q., Yan, L., Dong, J., Zhang, H., Li, L., Sun, L., Pan, N. , Xu
814 X, Tang F, Zhang J, Qiao J, Wang X.. (2018). A single-cell RNA-seq survey of the
815 developmental landscape of the human prefrontal cortex. *Nature* 555, 524-528.

816 Zufferey F, Sherr EH, Beckmann ND, Hanson E, Maillard AM, Hippolyte L, Mace A, Ferrari
817 C, Kutilik Z, Andrieux J, Aylward E, Barker M, Bernier R, Bouquillon S, Conus P,
818 Delobel B, Faucett WA, Goin-Kochel RP, Grant E, Harewood L, Hunter JV, Lebon S,
819 Ledbetter DH, Martin CL, Mannik K, Martinet D, Mukherjee P, Ramocki MB, Spence
820 SJ, Steinman KJ, Tjernagel J, Spiro JE, Raymond A, Beckmann JS, Chung WK,
821 Jacquemont S. 2012. A 600 kb deletion syndrome at 16p11.2 leads to energy imbalance
822 and neuropsychiatric disorders. *J Med Genet*. 49:660–668

823

824

825